ARTICLE

https://doi.org/10.1038/s41586-018-0784-9

L1 drives IFN in senescent cells and promotes age–associated inflammation

Marco De Cecco[1], Takahiro Ito[1], Anna P. Petrashen[1], Amy E. Elias[1], Nicholas J. Skvir[1], Steven W. Criscione[1], Alberto Caligiana[1,9], Greta Brocculi[1,9], Emily M. Adney[2,3], Jef D. Boeke[2], Oanh Le[4], Christian Beauséjour[4], Jayakrishna Ambati[5], Kameshwari Ambati[5], Matthew Simon[6], Andrei Seluanov[6], Vera Gorbunova[6], P. Eline Slagboom[7], Stephen L. Helfand[1], Nicola Neretti[1,8] & John M. Sedivy[1]*

Retrotransposable elements are deleterious at many levels, and the failure of host surveillance systems for these elements can thus have negative consequences. However, the contribution of retrotransposon activity to ageing and age–associated diseases is not known. Here we show that during cellular senescence, L1 (also known as LINE–1) retrotransposable elements become transcriptionally derepressed and activate a type–I interferon (IFN–I) response. The IFN–I response is a phenotype of late senescence and contributes to the maintenance of the senescence–associated secretory phenotype. The IFN–I response is triggered by cytoplasmic L1 cDNA, and is antagonized by inhibitors of the L1 reverse transcriptase. Treatment of aged mice with the nucleoside reverse transcriptase inhibitor lamivudine downregulated IFN–I activation and age–associated inflammation (inflammaging) in several tissues. We propose that the activation of retrotransposons is an important component of sterile inflammation that is a hallmark of ageing, and that L1 reverse transcriptase is a relevant target for the treatment of age–associated disorders.

The activity of retrotransposable elements (RTEs) can promote aberrant transcription, alternative splicing, insertional mutagenesis, DNA damage and genome instability[1]. RTE-derived sequences comprise up to two-thirds of the human genome[2], although the vast majority were active millions of years ago and are no longer intact. The only human RTE capable of autonomous retrotransposition is the long-interspersed element-1 (L1, also known as LINE-1). However, germline activity of L1 is a major source of human structural polymorphisms[3]. Increasing evidence points to RTE activation in some cancers, in the adult brain, and during ageing[4–7]. Cellular defences include heterochromatinization of the elements, small RNA pathways that target the transcripts, and antiviral innate immunity mechanisms[8]. Somatic activation of RTEs with age is conserved in yeast and *Drosophila* and reducing RTE activity has beneficial effects[8].

Activation of L1 and IFN–I in cellular senescence

We show here that L1 transcription is activated exponentially during replicative senescence of human fibroblasts, increasing 4–5-fold by 16 weeks after cessation of proliferation, which we refer to as late senescence (Fig. 1a, Extended Data Fig. 1a–e). Several quantitative reverse transcription PCR (RT–qPCR) primer pairs were designed to detect evolutionarily recent L1 elements (L1HS–L1PA5; Fig. 1b, Extended Data Fig. 1h). Levels of L1 poly(A)$^+$ RNA increased 4–5-fold in late replicatively senescent cells in the sense but not antisense direction throughout the entire element (Fig. 1c). Sanger sequencing of long-range RT–PCR amplicons (Fig. 1b) identified 224 elements that were dispersed throughout the genome; one-third (75, 33.5%) of these were L1HS, of which 19 (25.3%, 8.5% of total) were intact (annotated to be free of open-reading frame (ORF)-inactivating mutations; Extended Data Fig. 1f, g). We also performed 5′ rapid amplification of cDNA ends (RACE) with the same primers and found that most L1 transcripts upregulated in senescent cells initiated within or near the 5′ untranslated region (UTR) (Extended Data Fig. 2).

L1 elements can stimulate an IFN-I response[9]. We found that α-family interferons (*IFNA* gene cluster on chromosome 9, see Methods) *IFNA* and *IFNB1* were induced to high levels in late senescent cells (Fig. 1d, Extended Data Fig. 1i). Cellular senescence proceeds through an early DNA damage-response phase followed by the senescence-associated secretory phenotype (SASP) response[10]. We document here a third and even later phase, characterized by the upregulation of L1 and an IFN-I response (Fig. 1e), which has not been previously noted, probably because most studies have focused on earlier times. Whole transcriptome RNA sequencing (RNA-seq) analysis confirmed that the SASP and IFN-I responses are temporally distinct (Extended Data Fig. 3). The late phase of L1 activation and IFN-I induction was also observed in oncogene-induced senescence (OIS) and stress-induced premature senescence (SIPS) (Fig. 1e, Extended Data Fig. 1j, k).

Mechanisms of L1 activation

To explore how surveillance fails during senescence, we examined three factors: TREX1, RB1 and FOXA1. TREX1 is a 3′ exonuclease that degrades foreign invading DNAs and its loss has been associated with the accumulation of cytoplasmic L1 cDNA[11]. We found that the expression of TREX1 was markedly decreased in senescent cells (Extended Data Fig. 4a). RB1 has been shown to bind to repetitive elements, including L1 elements, and promote their heterochromatinization[12]. We found that the expression of RB1 declined strongly in senescent cells (Fig. 2a), whereas that of other RB family members (*RBL1* and *RBL2*) did not change (Extended Data Fig. 4b). RB1 enrichment in the 5′ UTR of L1 elements was evident in proliferating cells, decreased in early senescence and became undetectable at later times

[1]Department of Molecular Biology, Cell Biology and Biochemistry, Brown University, Providence, RI, USA. [2]Institute for Systems Genetics and Department of Biochemistry and Molecular Pharmacology, NYU Langone Health, New York, NY, USA. [3]McKusick-Nathans Institute of Genetic Medicine, Johns Hopkins University School of Medicine, Baltimore, MD, USA. [4]Centre de Recherche CHU Ste-Justine, and Department of Pharmacology and Physiology, Université de Montréal, Montréal, Québec, Canada. [5]Center for Advanced Vision Science and Department of Ophthalmology, University of Virginia School of Medicine, Charlottesville, VA, USA. [6]Department of Biology, University of Rochester, Rochester, NY, USA. [7]Department of Molecular Epidemiology, Leiden University Medical Centre, Leiden, The Netherlands. [8]Center for Computational Molecular Biology, Brown University, Providence, RI, USA. [9]Present address: Department of Pharmacy and Biotechnology, University of Bologna, Bologna, Italy. *e-mail: john_sedivy@brown.edu

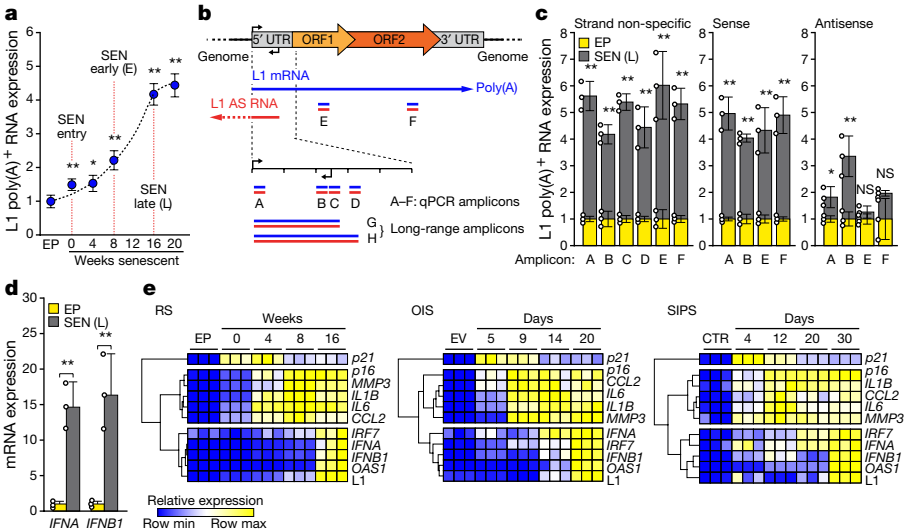

Fig. 1 | Activation of L1, IFN-I and SASP in senescent cells. Gene expression was assessed by RT–qPCR. Poly(A)-purified RNA was used in all L1 assays. **a**, Time course of L1 activation. *P* values were calculated relative to the early passage (EP) control. **b**, Schematic of L1 RT–PCR strategy. Blue, sense; red, antisense (AS). For primer specificity, see Extended Data Fig. 1f–h; for primer design, see Methods. Primers for amplicon F were used in **a** and **e**. **c**, Strand-specific L1 transcription was assessed using amplicons A–F. Transcription from the 5′ UTR antisense promoter was also detected. 'SEN (L)' denotes late senescence (16 weeks). **d**, Induction of *IFNA* and *IFNB1* mRNA levels in human fibroblasts. **e**, The temporal induction of genes associated with DNA damage (*p21* and *p16*, also known as *CDKN1A* and *CDKN2A*, respectively), SASP (*IL1B*, *CCL2*, *IL6* and *MMP3*), and the IFN-I response (*IRF7*, *IFNA*, *IFNB1* and *OAS1*). Row clustering was calculated as 1 − Pearson correlation. OIS, oncogene induced senescence (elicited by Ha-RAS infection); RS, replicative senescence; SIPS, stress-induced premature senescence (gamma irradiation). Controls: EP, early passage; EV, empty vector infected; CTR, non-irradiated. $n = 3$ independent biological samples, repeated in two independent experiments. Data are mean ± s.d. NS, not significant; $*P \leq 0.05$, $**P \leq 0.01$, unpaired two-sided *t*-test. Exact *P* values can be found in the accompanying Source Data.

(Fig. 2a). This coincided with a decrease of histone 3 Lys9 trimethylation (H3K9me3) and H3K27me3 marks in these regions (Extended Data Fig. 4c).

To identify factors that interact with the L1 5′ UTR, we examined the ENCODE chromatin-immunoprecipitation followed by sequencing (ChIP–seq) database and found that the pioneering transcription factor FOXA1 binds to this region in several cell lines (Extended Data Fig. 4d). FOXA1 is upregulated in senescent cells[13] and bound to the central region of the L1 5′ UTR (Fig. 2b). Using transcriptional reporters, we found that deletion of the FOXA1-binding site decreased both sense and antisense transcription from the L1 5′ UTR[14] (Extended Data Fig. 4e). Hence, the observed misregulation of these three factors in senescent cells could promote the activation of L1 by three additive mechanisms: loss of RB1 by relieving heterochromatin repression; gain of FOXA1 by activating the L1 promoter; and loss of TREX1 by compromising the removal of L1 cDNA.

We thus tested the effects of manipulating RB1, FOXA1 or TREX1 expression in fully senescent cells using lentiviral vectors (Extended Data Fig. 5a, b). Ectopic expression of RB1 suppressed the increased expression of L1, *IFNA* and *IFNB1* in senescent cells, whereas knockdown of RB1 further enhanced their expression (Fig. 2d). RB1 overexpression also restored its occupancy of the L1 5′ UTR (Fig. 2c). Conversely, knockdown of FOXA1 reduced its binding to the L1 5′ UTR (Extended Data Fig. 4f) and decreased the expression of L1, *IFNA* and *IFNB1*, whereas overexpression of FOXA1 increased the expression of L1, *IFNA* and *IFNB1* (Fig. 2e). Congruent results were also obtained by manipulating TREX1 (Fig. 2g). Hence, each of these factors had a tangible effect on the regulation of L1 and the IFN-I response in senescent cells.

Single or double interventions targeted at these factors elicited only modest changes in L1 and IFN-I expression in growing early passage cells. Although some of these effects were statistically significant, they were overshadowed by a triple intervention (3×) of RB1 and TREX1 knockdowns combined with FOXA1 overexpression, which resulted in a large induction of L1 and IFN-I expression (Fig. 2f, Extended Data Figs. 4g–i, 5c). Hence, in normal healthy cells all three effectors have to be compromised to unleash L1 effectively.

Consequences of L1 activation

To assess IFN-I activation by L1 in more detail, we examined the expression of 84 genes in this pathway using PCR arrays. We observed a widespread response, with most genes being upregulated (Fig. 2h, Extended Data Fig. 4j, k): 68% (57 out of 84) were significantly upregulated in senescent cells, and 52% (44 out of 84) were upregulated in 3× cells. These data verify and further extend the RNA-seq transcriptomic analysis (Extended Data Fig. 3).

Some nucleoside reverse transcriptase inhibitors (NRTIs) developed against HIV have been found to also inhibit L1 reverse transcriptase activity[15]. We also developed short hairpin RNAs (shRNAs) against L1, two of which reduced transcript levels by 40–50% and 70–90% in deeply senescent and 3× cells, respectively (Extended Data Fig. 5g). Amounts of ORF1 protein were correspondingly reduced in deeply senescent cells (Extended Data Fig. 5h). Finally, the shRNAs also reduced the retrotransposition of recombinant L1 reporter constructs (Extended Data Fig. 5k).

Cells devoid of TREX1 display cytoplasmic L1 DNA, the accumulation of which can be inhibited with NRTIs[11]. Although the lack of BrdU incorporation is a canonical feature of senescent cells (Extended Data Fig. 1b), longer term labelling revealed DNA species that were predominantly cytoplasmic and highly enriched for L1 sequences (Extended Data Fig. 6a, b). The synthesis of cytoplasmic L1 DNA could be almost completely blocked by the NRTI lamivudine (also known as 3TC) or by shRNA to L1 (Fig. 3a, c). An antibody to DNA–RNA hybrids detected a cytoplasmic signal in senescent cells that largely colocalized with ORF1 protein and turned into a single-stranded DNA (ssDNA) signal after RNase digestion (Extended Data Fig. 6c). Analysis of BrdU-labelled L1 sequences in senescent cells showed them to be localized throughout the L1 element (Extended Data Fig. 6d, e). A relative increase of L1HS sequences in total cellular DNA can also be detected by a qPCR assay[6,16]. 3TC in the range of 7.5 to 10 μM completely blocked this increase in senescent cells and also quenched the activity of a L1 retrotransposition reporter (Extended Data Fig. 5d, e).

L1 knockdown with shRNA or treatment of cells with 3TC significantly reduced interferon levels, as well as reducing the IFN-I response more broadly in both late senescent and 3× cells (Fig. 3b, Extended

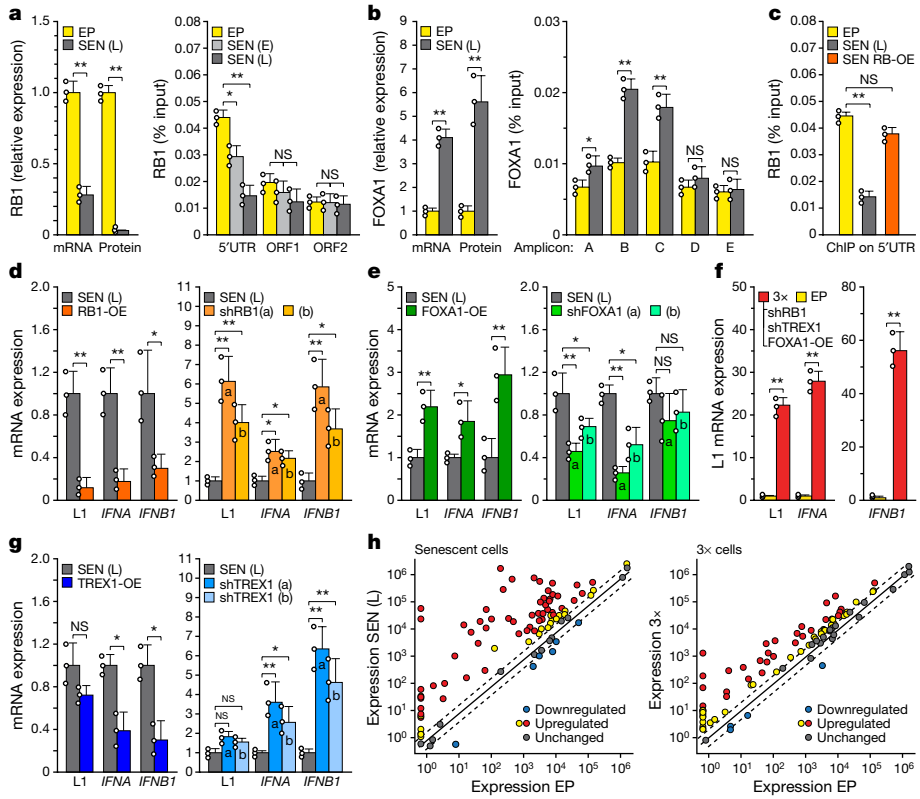

Fig. 2 | Regulation of L1 activation and IFN-I induction. a, **b**, Expression and ChIP of RB1 (**a**) and FOXA1 (**b**). Left, expression was measured by RT–qPCR and immunoblotting. Right, binding to L1 elements was assessed with ChIP–qPCR. For primer locations see Fig. 1b. RB1: 5′ UTR, ORF1 and ORF2, primers for amplicons A, E and F, respectively. FOXA1: primers for amplicons A–E. qPCR was normalized to input chromatin. 'SEN (E)' denotes early senescence (8 weeks). For gel source data, see Supplementary Fig. 1. **c**, RB1 was overexpressed (OE), and its binding to 5′ UTR of L1 elements was assessed by ChIP–qPCR (amplicon A). **d**, **e**, **g**, RB1 (**d**), FOXA1 (**e**) or TREX1 (**g**) were overexpressed or ablated with shRNAs (shRB1, shFOXA1 or shTREX1), and the effects on mRNA expression of L1, *IFNA* and *IFNB1* were determined by RT–qPCR of poly(A)-purified RNA. In all cases, lentiviral vectors were used to deliver the interventions directly into senescent cells at 12 weeks (Extended Data Fig. 1a, point D), and cells were collected for analysis 4 weeks later (point E, 16 weeks). Controls were uninfected senescent cells obtained at the same time (point E, 16 weeks). Two distinct shRNAs (a and b) were used for each gene. Primers for amplicon F were used for L1. **f**, Activation of L1, *IFNA* and *IFNB1* mRNA expression after the triple intervention (3×) using shRB1 (a), shTREX1 (a) and FOXA1-OE in early passage cells. Lentiviral infections were performed sequentially with drug selections at each step (shRB1, puromycin; shTREX1, hygromycin; FOXA1-OE, blasticidin). **h**, Expression of IFN-I pathway genes was determined with the RT^2 Profiler PCR array (Qiagen). Normalized mean expression is shown for all 84 genes in the array. Red symbols denote significantly upregulated genes. Dashed lines demarcate the ±twofold range. $n = 3$ independent biological samples, repeated in two independent experiments (**a**, **b**, **h**); $n = 3$ independent experiments (**c**–**g**). Data are mean ± s.d. $^*P \leq 0.05$, $^{**}P \leq 0.01$, unpaired two-sided *t*-test. Exact *P* values can be found in the accompanying Source Data.

Data Fig. 7a). 3TC in the range of 7.5 to 10 μM optimally inhibited the IFN-I response, and was the most effective of four NRTIs tested (Extended Data Fig. 5f, j). The relative efficacies of the NRTIs are consistent with their ability to inhibit human L1 reverse transcriptase[15]. 3TC also antagonized the IFN-I response in other forms of senescence, OIS and SIPS (Fig. 3e).

We passaged cells in the continuous presence of 3TC from the proliferative phase into deep senescence. 3TC did not significantly affect the timing of entry into senescence, induction of p21 or p16, or the early SASP response (such as upregulation of IL-1β (Fig. 3f, Extended Data Fig. 7b). However, the magnitude of the later SASP response (such as the induction of CCL2, IL-6 and MMP3) was significantly dampened. Treatment with L1 shRNA also reduced the expression levels of IL-6 and MMP3 in late senescent cells (Extended Data Fig. 6f). Hence, although L1 activation and the ensuing IFN-I response are relatively late in onset, they contribute importantly to the mature SASP and pro-inflammatory phenotype of senescent cells.

3TC did not affect L1 transcript levels (Extended Data Fig. 5i), suggesting that the IFN-I response is triggered by L1 cDNA. As predicted by this model, knockdown of the cytosolic DNA-sensing pathway components cGAS or STING[17] inhibited the IFN-I response in both late senescent and 3× cells (Extended Data Figs. 5l, 7c, d), and also downregulated the SASP response in late senescent cells (Extended Data Fig. 7e).

NRTIs alkyl-modified at the 5′ ribose position cannot be phosphorylated and hence do not inhibit reverse transcriptase enzymes; however, they possess intrinsic anti-inflammatory activity by inhibiting P2X7-mediated events that activate the NLRP3 inflammasome pathway[18]. Tri-methoxy-3TC (also known as Kamuvudine-9 and K-9), at 10 μM or 100 μM, did not inhibit the IFN-I response in either late senescent or 3× cells (Extended Data Fig. 7f). Hence, the effect of 3TC on the IFN-I pathway requires reverse transcriptase inhibition. At high concentrations (100 μM), K-9 had some inhibitory activity on markers of inflammation, as reported previously[18] (Extended Data Fig. 7g).

To test the role of interferon signalling in SASP, we inactivated the IFNα and IFNβ receptor genes (*IFNAR1* and *IFNAR2*) using CRISPR–Cas9. Effective ablation of IFN-I signalling was achieved in both early passage and deep senescent cells (Extended Data Fig. 5m). In both replicative and SIPS forms of senescence, loss of interferon signalling antagonized late (CCL2, IL-6 and MMP3) but not early (IL-1β) SASP markers (Fig. 3d). This further demonstrates that IFN-I signalling contributes to the establishment of a full and mature SASP response in senescent cells.

Activation of L1 in human and mouse tissues

Activation of L1 expression in human cancers has been detected with an ORF1 antibody[4]. The same reagent showed widespread ORF1

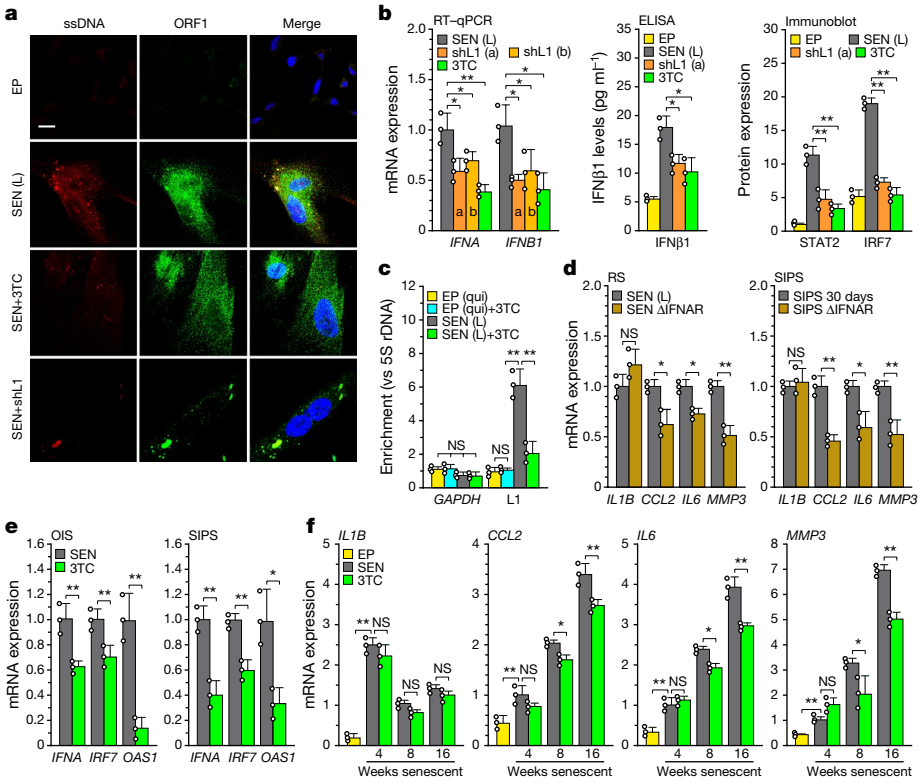

Fig. 3 | Ablation of L1 relieves IFN-I activation and blunts the SASP response. a, Cells were examined by immunofluorescence microscopy using antibodies against ssDNA or L1 ORF1 protein. Note the bright cytoplasmic ssDNA puncta in senescent cells that colocalized with prominent puncta of ORF1. The experiment was independently repeated three times with similar results. Scale bar, 10 μm. **b**, Senescent cells were treated with L1 shRNAs (using lentiviral vectors as described in Fig. 2d, e, g) or with 3TC (7.5 μM) between 12 and 16 weeks of senescence. Effects on the IFN-I response were determined by RT–qPCR, ELISA or immunoblotting. For gel source data, see Supplementary Fig. 1. **c**, Cells were labelled with BrdU for 2 weeks (with or without 7.5 μM 3TC), labelled DNA was immunoprecipitated, and its L1 sequence content was quantified using a TaqMan multiplex qPCR assay[16] (Fig. 1b, amplicon F). 'EP (qui)' denotes early passage quiescent cells. **d**, Left, replicatively senescence cells. *IFNAR1* and *IFNAR2* genes were mutagenized using the CRISPR–Cas9 system delivered with lentivirus vectors directly into senescent cells. As with shRNA interventions, cells were infected at 12 weeks and collected at 16 weeks of senescence (Fig. 2d, e, g, Methods). Right, SIPS cells. CRISPR–Cas9 intervention was performed in early passage cells and a validated clone was irradiated to induce SIPS. **e**, OIS (left) and SIPS (right) were induced as in Fig. 1d and cells were collected 20 (OIS) or 30 (SIPS) days later. 3TC (7.5 μM) was present throughout. IFN-I gene expression (*IFNA*, *IRF7* and *OAS1*) was measured by RT–qPCR **f**, Cells were serially passaged into replicative senescence with 3TC (10 μM) present throughout, and the temporal induction of SASP response genes (*IL1B*, *CCL2*, *IL6* and *MMP3*) was assessed. $n = 3$ independent experiments (**b**–**d**, **f**); $n = 3$ independent biological samples, repeated in two independent experiments (**e**). Data are mean ± s.d. $^*P \leq 0.05$, $^{**}P \leq 0.01$, unpaired two-sided *t*-test (**b**, **d**–**f**) or one-way ANOVA with Tukey's multiple comparisons test (**c**). Exact *P* values can be found in the accompanying Source Data.

expression in both senescent and 3× cells (Extended Data Fig. 8a, c, f). In skin biopsies of aged human individuals, we found that 10.7% of dermal fibroblasts were positive for the senescence marker p16, which is in the range documented in ageing primates[19] (Extended Data Fig. 8b, d, f, h). Some of the p16-positive dermal fibroblasts were also positive for ORF1 (10.3%). Notably, we did not observe ORF1 in the absence of p16 expression. We also detected, at the single-cell level, the presence of phosphorylated STAT1, consistent with the presence of interferon signalling in the tissue microenvironment[20] (Extended Data Fig. 8b, e, g). Hence, a fraction of senescent cells in normal human individuals displays activation of L1, consistent with these events accumulating during the progression of senescence.

We next examined mice and found that L1 mRNA was progressively upregulated with age in several tissues (Extended Data Fig. 10g). The detected L1 RNA sequences were predominantly sense strand, represented throughout the element, and all three active L1 families were detectable (Extended Data Fig. 6g, h). At the protein level, the frequency of L1 ORF1-positive cells increased in tissues with age (Fig. 4a). Regions of ORF1 staining colocalized with the activity of senescence-associated β-galactosidase (SA-β-Gal) (Fig. 4b). Notably, we found that several IFN-I response genes (*Ifna*, *Irf7* and *Oas1*) as well as pro-inflammatory and SASP markers (*Il6*, *Mmp3* and *Pai1* (also known as *Serpine1*)) were upregulated in the tissues of old (26 months) mice (Fig. 4c, Extended Data Fig. 9). We also observed an increase in L1 expression and IFN-I response genes (*Ifna* and *Oas1*) in an experimentally induced model of cellular senescence (young mice subjected to sublethal irradiation; Fig. 4d).

We treated old mice (26 months) for two weeks with 3TC (administered in water at human therapeutic doses) and found a broad and significant downregulation of the IFN-I response and alleviation of the SASP pro-inflammatory state (Fig. 4c; see Extended Data Fig. 9 and Supplementary Table 7 for the full dataset). The expression of L1 and *p16* (also known as *Cdkn2a*) mRNA was weakly downregulated, but in most cases did not reach statistical significance. K-9 did not affect either the IFN-I or the SASP responses. Immunofluorescence analysis of tissue sections confirmed that senescent cells expressed SASP markers, and ORF1-expressing cells activated IFN-I signalling (Extended Data Fig. 10a–c). Treatment with 3TC significantly reduced both the IFN-I and SASP responses, but not L1 expression or the presence of senescent cells. Hence, NRTIs can be categorized as 'senostatic' agents, in contrast to 'senolytic' treatments that remove senescent cells from tissues[21,22].

Decreased adipogenesis[23] and thermogenesis[24] are features of natural ageing and both were increased in old mice by 2 weeks of 3TC treatment (Extended Data Fig. 10d–f). Longer term treatments (from 20 to 26 months of age) were effective at opposing several known phenotypes

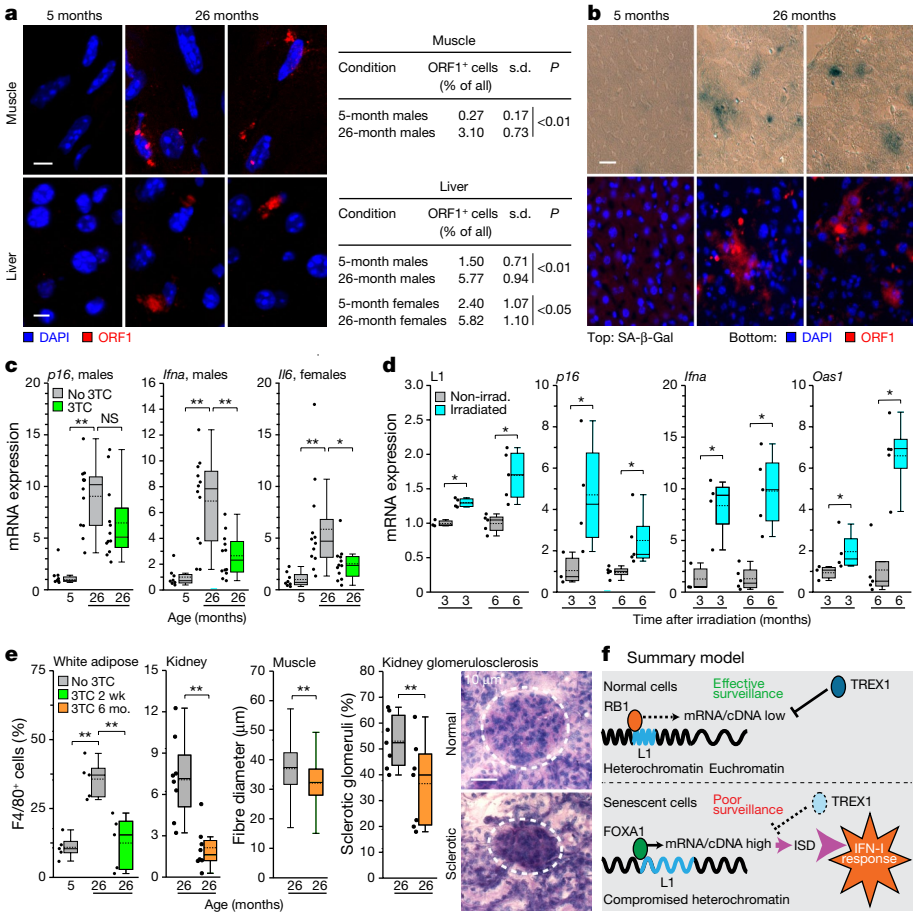

Fig. 4 | L1 elements are activated with age in mouse tissues and the IFN-I pro-inflammatory response is relieved by NRTI treatment. a, Presence of L1 ORF1 protein in tissues was examined by immunofluorescence microscopy. Quantification of ORF1-expressing cells is shown in the right panel; 3 mice and at least 200 cells per mouse were scored for each condition. Scale bar, 4 μm. **b**, Activation of L1 in senescent cells was examined by co-staining for SA-β-Gal activity and ORF1 protein by immunofluorescence (male liver, 5 and 26 months). Scale bar, 4 μm. The experiment was repeated three times independently with similar results. **c**, Mice were administered 3TC (2 mg ml^{-1}) in drinking water at the indicated ages for two weeks and euthanized after treatment. Expression of *p16*, an IFN-I response gene (*Ifna*), and a marker of a pro-inflammatory state (*Il6*) were assessed in aged adipose tissue by RT–qPCR. See Extended Data Fig. 9 for additional tissues and genes. The box plots in **c** and all subsequent panels show the range of the data (whiskers), 25th and 75th percentiles (box), means (dashed line), and medians (solid line). Each point represents one mouse. $n = 8$ mice at 5 months; $n = 12$ mice at 26 months; $n = 6$ mice at 29 months. **d**, Six-month-old mice were non-lethally irradiated and the expression of L1, *p16* and representative IFN-I response genes (*Ifna*, *Oas1*) was assessed by RT–qPCR at the indicated times after irradiation in adipose tissue of male mice. Non-irradiated, $n = 3$ mice at 3 months, $n = 5$ mice at 6 months; irradiated, $n = 4$ mice at 3 months, $n = 5$ mice at 6 months. **e**, Macrophage infiltration into white adipose tissue and kidney was scored as F4/80-positive cells (percentage of total nuclei). $n = 5$ mice (adipose); $n = 8$ mice (kidney). Skeletal muscle fibre diameter was measured (Methods) and plotted as an aggregate box plot. $n = 5$ mice per group, 500 fibres total. Glomerulosclerosis was scored in periodic acid-Shiff (PAS)-stained sections (Methods) as the sum of all glomeruli with a score of 3 or 4 divided by the total. $n = 7$ mice per group, 40 glomeruli per animal. 3TC treatment was 2 weeks for white adipose and 6 months (20–26 months) for other tissues. Dashed circle demarcates a single glomerulus. Scale bar, 50 μm. **f**, Breakdown of L1 surveillance mechanisms leads to chronic activation of the IFN-I response. ISD, interferon-stimulatory DNA pathway. $^*P \leq 0.05$, $^{**}P \leq 0.01$, unpaired two-sided *t*-test (**a**, **d**, **e**), or one-way ANOVA with Tukey's multiple comparisons test (**c**, **e** white adipose). Exact *P* values can be found in the accompanying Source Data.

of ageing: macrophage infiltration of tissues (a hallmark of chronic inflammation[23,25]), glomerulosclerosis of the kidney[26], and skeletal muscle atrophy[27] (Fig. 4e). Macrophage infiltration of white adipose tissue was especially responsive, returning to youthful (5-month) levels with only 2 weeks of 3TC treatment.

The activation of endogenous L1 elements and the ensuing robust activation of an IFN-I response is a phenotype of senescent cells, including naturally occurring senescent cells in tissues. This phenotype evolves progressively during the senescence response and seems to be an important, but until now unappreciated, component of SASP. We show that the expression of three regulators, RB1, FOXA1 and TREX1, changes during senescence, and that these changes are both sufficient and necessary to allow the transcriptional activation of L1 elements (Fig. 4f). Hence, several surveillance mechanisms need to be defeated to unleash L1, which underscores the importance of keeping these elements repressed in somatic cells. We anticipate that future work will uncover additional mechanisms and failure points that can lead to the activation of endogenous RTEs.

The activation of innate immune signalling in response to L1 activation during cellular senescence and ageing proceeds through the interferon-stimulatory DNA pathway. Cytoplasmic DNA can originate from several sources, such as mitochondrial DNA released from stressed mitochondria[28] or cytoplasmic chromatin fragments released from damaged nuclei[29,30]. Our results suggest that L1 cDNA is an important inducer of IFN-I in senescent cells. Notably, NRTI treatment effectively antagonized not only the IFN-I response but also more broadly reduced age-associated chronic inflammation in multiple tissues.

Sterile inflammation, also known as 'inflammaging', is a hallmark of ageing and a contributing factor to many age-related diseases[31,32].

We propose that the activation of L1 elements (and possibly other RTEs in the mouse) promotes age-associated inflammation, and that the L1 reverse transcriptase is a relevant target for the development of drugs to treat age-associated disorders.

Online content

Any methods, additional references, Nature Research reporting summaries, source data, statements of data availability and associated accession codes are available at https://doi.org/10.1038/s41586-018-0784-9

Received: 20 December 2016; Accepted: 2 November 2018;
Published online 6 February 2019.

1. Huang, C. R., Burns, K. H. & Boeke, J. D. Active transposition in genomes. *Annu. Rev. Genet.* **46**, 651–675 (2012).
2. de Koning, A. P., Gu, W., Castoe, T. A., Batzer, M. A. & Pollock, D. D. Repetitive elements may comprise over two-thirds of the human genome. *PLoS Genet.* **7**, e1002384 (2011).
3. Hancks, D. C. & Kazazian, H. H., Jr. Active human retrotransposons: variation and disease. *Curr. Opin. Genet. Dev.* **22**, 191–203 (2012).
4. Rodić, N. et al. Long interspersed element-1 protein expression is a hallmark of many human cancers. *Am. J. Pathol.* **184**, 1280–1286 (2014).
5. Erwin, J. A., Marchetto, M. C. & Gage, F. H. Mobile DNA elements in the generation of diversity and complexity in the brain. *Nat. Rev. Neurosci.* **15**, 497–506 (2014).
6. De Cecco, M. et al. Genomes of replicatively senescent cells undergo global epigenetic changes leading to gene silencing and activation of transposable elements. *Aging Cell* **12**, 247–256 (2013).
7. Van Meter, M. et al. SIRT6 represses LINE1 retrotransposons by ribosylating KAP1 but this repression fails with stress and age. *Nat. Commun.* **5**, 5011 (2014).
8. Kreiling, J. A. et al. in *Human Retrotransposons in Health and Disease* (ed. Cristofari, G.) 297–321 (Springer International, New York, 2017).
9. Volkman, H. E. & Stetson, D. B. The enemy within: endogenous retroelements and autoimmune disease. *Nat. Immunol.* **15**, 415–422 (2014).
10. Salama, R., Sadaie, M., Hoare, M. & Narita, M. Cellular senescence and its effector programs. *Genes Dev.* **28**, 99–114 (2014).
11. Thomas, C.A. et al. Modeling of TREX1-dependent autoimmune disease using human stem cells highlights L1 accumulation as a source of neuroinflammation. *Cell Stem Cell* **21**, 319–331.e8 (2017).
12. Ishak, C. A. et al. An RB-EZH2 complex mediates silencing of repetitive DNA sequences. *Mol. Cell* **64**, 1074–1087 (2016).
13. Li, Q. et al. FOXA1 mediates $p16^{INK4a}$ activation during cellular senescence. *EMBO J.* **32**, 858–873 (2013).
14. Denli, A. M. et al. Primate-specific ORF0 contributes to retrotransposon-mediated diversity. *Cell* **163**, 583–593 (2015).
15. Dai, L., Huang, Q. & Boeke, J. D. Effect of reverse transcriptase inhibitors on LINE-1 and Ty1 reverse transcriptase activities and on LINE-1 retrotransposition. *BMC Biochem.* **12**, 18 (2011).
16. Coufal, N. G. et al. L1 retrotransposition in human neural progenitor cells. *Nature* **460**, 1127–1131 (2009).
17. Dhanwani, R., Takahashi, M. & Sharma, S. Cytosolic sensing of immuno-stimulatory DNA, the enemy within. *Curr. Opin. Immunol.* **50**, 82–87 (2018).
18. Fowler, B. J. et al. Nucleoside reverse transcriptase inhibitors possess intrinsic anti-inflammatory activity. *Science* **346**, 1000–1003 (2014).
19. Herbig, U., Ferreira, M., Condel, L., Carey, D. & Sedivy, J. M. Cellular senescence in aging primates. *Science* **311**, 1257 (2006).
20. Coppé, J. P., Desprez, P. Y., Krtolica, A. & Campisi, J. The senescence-associated secretory phenotype: the dark side of tumor suppression. *Annu. Rev. Pathol.* **5**, 99–118 (2010).
21. Chang, J. et al. Clearance of senescent cells by ABT263 rejuvenates aged hematopoietic stem cells in mice. *Nat. Med.* **22**, 78–83 (2016).
22. Zhu, Y. et al. The Achilles' heel of senescent cells: from transcriptome to senolytic drugs. *Aging Cell* **14**, 644–658 (2015).
23. Tchkonia, T. et al. Fat tissue, aging, and cellular senescence. *Aging Cell* **9**, 667–684 (2010).
24. Mattson, M. P. Perspective: Does brown fat protect against diseases of aging? *Ageing Res. Rev.* **9**, 69–76 (2010).
25. Frasca, D. & Blomberg, B. B. Inflammaging decreases adaptive and innate immune responses in mice and humans. *Biogerontology* **17**, 7–19 (2016).
26. Baker, D. J. et al. Naturally occurring $p16^{Ink4a}$-positive cells shorten healthy lifespan. *Nature* **530**, 184–189 (2016).
27. Baker, D. J. et al. Clearance of $p16^{Ink4a}$-positive senescent cells delays ageing-associated disorders. *Nature* **479**, 232–236 (2011).
28. West, A. P. & Shadel, G. S. Mitochondrial DNA in innate immune responses and inflammatory pathology. *Nat. Rev. Immunol.* **17**, 363–375 (2017).
29. Dou, Z. et al. Cytoplasmic chromatin triggers inflammation in senescence and cancer. *Nature* **550**, 402–406 (2017).
30. Takahashi, A. et al. Downregulation of cytoplasmic DNases is implicated in cytoplasmic DNA accumulation and SASP in senescent cells. *Nat. Commun.* **9**, 1249 (2018).
31. Franceschi, C. & Campisi, J. Chronic inflammation (inflammaging) and its potential contribution to age-associated diseases. *J. Gerontol. A Biol. Sci. Med. Sci.* **69** (suppl. 1), S4–S9 (2014).
32. López-Otín, C., Blasco, M. A., Partridge, L., Serrano, M. & Kroemer, G. The hallmarks of aging. *Cell* **153**, 1194–1217 (2013).

Acknowledgements The following funding sources are acknowledged: M.D., Glenn/AFAR Postdoctoral Fellowship, NIH P20 GM119943 COBRE pilot award; T.I., NIH F31 AG043189; A.P.P. and A.E.E., NIH T32 AG041688; S.W.C., NIH F31 AG050365; A.C. and G.B., Biotechnology and Sport Medicine Fellowships, School of Pharmacy, University of Bologna, Bologna, Italy; E.M.A. and J.D.B., NIH P01 AG051449; C.B., Canadian Institute of Health Research MOP-102709; J.A., NIH DP1 GM114862, R01 EY022238, R01 EY024068, R01 EY028027, John Templeton Foundation Grant ID 60763; M.S., A.S. and V.G., NIH R01 AG046320, R01 AG027237, R01 AG047200, P01 AG051449, Life Extension Foundation; S.L.H., NIH R37 AG016667, R01 AG024353, P01 AG051449, Glenn-AFAR Breakthroughs in Gerontology Award; N.N., NIH R01 AG050582, P20 GM109035; J.M.S., NIH R37 AG016694, P01 AG051449. We are grateful to A. Maier, M. Waaijer, R. Westendorp and the participants of the Leiden Longevity Study (LLS) for assistance with the human specimens. We thank D. Baker for guidance with the glomerulosclerosis assay. The biomaterials collection of the LLS (P.E.S., principal investigator) was supported by the Netherlands Genomics Initiative of the Netherlands Organization for Scientific Research (NWO), within the framework of the Netherlands Consortium of Healthy Ageing (NCHA, 050-060-810) and the Leiden University Medical Center.

Reviewer information *Nature* thanks D. Sinclair, J. van Deursen and the anonymous reviewer(s) for their contribution to the peer review of this work.

Author contributions J.M.S. conceived the study. J.M.S. and M.D. designed the experiments. M.D. and T.I. maintained cell cultures and performed lentiviral interventions. M.D. performed RT–qPCR in cell culture and mouse tissues with help from M.S. and G.B. T.I. and A.C. performed immunoblots. M.D. performed all immunofluorescence analyses. N.J.S., S.W.C. and A.E.E. did the bioinformatics and statistics. A.P.P. performed immunohistochemistry and tissue histology. E.M.A. generated and validated antibodies against mouse ORF1. O.L. irradiated mice and collected tissues. J.A. and K.A. provided NRTI analogues. P.E.S. provided human samples. J.D.B., C.B., J.A., K.A., A.S., V.G., P.E.S., S.L.H., N.N. and J.M.S. contributed to personnel supervision, data interpretation and critical analysis. J.M.S. and M.D. wrote the manuscript with feedback from all authors.

Competing interests J.A. is a cofounder of iVeena Holdings, iVeena Delivery Systems, and Inflammasome Therapeutics, and has been a consultant for Allergan, Biogen, Boehringer-Ingelheim, Janssen, Olix Pharmaceuticals, and Saksin LifeSciences in a capacity unrelated to this work. J.A. and K.A. are named as inventors on patent applications on macular degeneration filed by the University of Kentucky or the University of Virginia. J.D.B. is a founder and Director of Neochromosome, Inc., the Center of Excellence for Engineering Biology, and CDI Labs, Inc. He serves on the Scientific Advisory Boards of Modern Meadow, Inc., Recombinetics, Inc., and Sample6, Inc.

Additional information
Extended data is available for this paper at https://doi.org/10.1038/s41586-018-0784-9.
Supplementary information is available for this paper at https://doi.org/10.1038/s41586-018-0784-9.
Reprints and permissions information is available at http://www.nature.com/reprints.
Correspondence and requests for materials should be addressed to J.M.S.
Publisher's note: Springer Nature remains neutral with regard to jurisdictional claims in published maps and institutional affiliations.

METHODS

Cell culture. Several different strains of normal human fibroblasts were used in this study. LF1 cells were derived from embryonic lung tissue as described[33]. These cells have been in continuous use in our laboratory since their isolation in 1996. Original samples frozen in 1996 and in continuous storage in our laboratory were recovered and used. IMR-90 and WI-38 cells were obtained from the ATCC. None of these cell lines is listed in the International Cell Line Authentication Committee (ICLAC) database. These normal fibroblast cell lines were cultured using physiological oxygen conditions (92.5% N_2, 5% CO_2, 2.5% O_2), in Ham's F-10 nutrient mixture (Thermo Scientific) with 15% fetal bovine serum (FBS; Hyclone). Medium was additionally supplemented with L-glutamine (2 mM), penicillin and streptomycin[34]. Cell cultures were periodically tested for mycoplasma contamination with MycoAlert Mycoplasma Detection Kit (Lonza).

To obtain replicatively senescent cells, LF1 cultures were serially propagated until proliferation ceased. At each passage, after reaching 80% confluence, cells were trypsinized and diluted 1:4. Hence each passage is equivalent to approximately two population doublings. In early passage cultures, the time between passages was constant at approximately 3 days. As cultures approached senescence, the time between passages gradually increased. An interval of 2–3 weeks indicated that the culture was in its penultimate passage. At this point, after reaching 80% confluence, the cells were replated at a 1:2 dilution, and this time was designated as the last passage (point A in Extended Data Fig. 1a). Some cell growth typically does occur in the next 2–3 weeks, but the cultures do not reach 80%. Under this experimental regimen, most of the cells in the culture enter senescence within a 3–4-week window centred roughly around the time of last passage (grey bar in Extended Data Fig. 1a). At point B (4 weeks), the cultures were trypsinized and replated as described[35] to eliminate a small fraction of persisting contact-inhibited cells. Cultures were again replated at point C (8 weeks).

OIS was elicited by infecting proliferating LF1 cells with pLenti CMV RasV12 Neo (gift from E. Campeau, Addgene plasmid 22259). Generation of lentiviral particles and the infection procedure are described below. At the end of the infection, cells were reseeded at 15–20% confluency and selected with G418 (250 μg ml^{-1}) maintained continuously until the end of the experiment. Medium was changed every 3 days until the cultures were harvested at the indicated time points. SIPS was elicited by X-ray irradiation with 20 Gy given at a rate of 87 cGy min^{-1} in one fraction using a caesium-137 gamma source (Nordion Gammacell 40). Cells were 15–20% confluent at the time of irradiation. Medium was changed immediately after irradiation, and at 3-day intervals thereafter. 293T cells (Clontech) were used to package lentivirus vectors and were cultured at 37 °C in DMEM with 10% FBS under normoxic conditions (air supplemented with 5% CO_2).

Nucleoside reverse transcriptase inhibitors. All NRTIs (lamivudine (3TC); zidovudine (also known as azidothymidine, AZT); abacavir, (ABC); emtricitabine (FTC)) used in this study were USP grade and obtained from Aurobindo Pharma. For Trizivir (TZV), its constituents (ABC, AZT and 3TC) were combined in the appropriate amounts. Kamuvudine-9 (K-9)[36] was provided by Inflammasome Therapeutics.

Mouse husbandry. Compliance with relevant ethical regulations and all animal procedures was reviewed and approved by the Brown University Institutional Animal Care and Use Committee. C57BL/6J mice of both sexes were obtained from the NIA Aged Rodent Colonies (https://www.nia.nih.gov/research/dab/aged-rodent-colonies-handbook) at 5 and 18 months of age. The 5-month-old mice were euthanized after a short (1-week) acclimatization period, a variety of tissues were collected, snap frozen in liquid nitrogen and stored at −80 °C. The 18-month-old mice were housed until they reached a desired age. Mice were housed in a specific pathogen-free AAALAC-certified barrier facility. All procedures were approved by the Brown University IACUC committee. Cages, bedding (Sani-chip hardwood bedding) and food (Purina Laboratory Chow 5010) were sterilized by autoclaving. Food and water (also sterilized) were provided ad libitum. A light–dark cycle of 12 h was used (7:00 on, 19:00 off). Temperature was maintained at 21 °C, and humidity at 50%. All mice were observed daily and weighed once per week. In a pilot experiment, three cohorts of ten mice each were treated with 3TC dissolved in drinking water (1.5 mg ml^{-1}, 2.0 mg ml^{-1}, 2.5 mg ml^{-1}) continuously from 18 months until euthanization at 24 months. The fourth (control) cohort was provided with the same water without drug. No significant differences in behaviour, weight or survival were observed between the four cohorts during the entire experiment. Once during the experiment (at 20 months of age) the mice were subjected to a single tail bleed of approximately 70 μl. The collected plasma was shipped to the University of North Carolina CFAR Clinical Pharmacology and Analytical Chemistry Core for analysis of 3TC. For the 2 mg ml^{-1} cohort, the concentration of 3TC in plasma averaged 7.2 μM. This dose of drug was chosen for further experiments to mimic the human HIV therapeutic dose (300 mg per day, 5–8 μM in plasma)[37]. For all experiments, mice were aged in house until they reached 26 months of age. They were then assigned randomly to two cohorts by a technician that was blinded to the appearance or other characteristics of the mice. One cohort was treated for 2 weeks with 2 mg ml^{-1} of 3TC in drinking water, and the other (control) cohort with same water without drug, administered in the same manner. At the end of the treatment period, all mice were euthanized and collected for tissues as described above. All mice in both cohorts were included in all subsequent analyses. The experiment was performed on separate occasions with male and female mice. Non-lethal total body irradiation (6 Gy) was performed as described previously[38] and tissue specimens were shipped to Brown University on dry ice.

PCR. The ABI ViiA 7 instrument (Applied Biosystems) was used for all experiments. qPCR of DNA was performed using the Taqman system (Applied Biosystems) as described previously[16]. Purified genomic DNA (100 pg) was used with the indicated primers (Supplementary Table 1). RT–qPCR of RNA was performed using the SYBR Green system (Applied Biosystems). Polyadenylated RNA was used in all experiments assessing transcription of L1 elements, and total RNA was used for all other genes. Total RNA was collected using the Trizol reagent (Invitrogen). Poly(A) RNA was isolated from total RNA using the NEBNext Poly(A) mRNA Magnetic Isolation Module (New England Biolabs). Total RNA (1 μg) or poly(A) RNA (10 ng) was reverse-transcribed into cDNA in 50-μl reactions using the Taqman kit (Applied Biosystems). To assess strand-specific transcription, the random primers in the reverse transcription reaction were substituted with a strand-specific primer to the target RNA. One microlitre of each reverse transcription reaction was used in subsequent qPCR reactions. *GAPDH* was used as the normalization control in experiments with human cells. The arithmetic mean of *Gapdh* and two additional controls (*Hsp90* (also known as *Hsp90ab1*) and *Gusb*) was used for normalization of RT–qPCR experiments with mouse tissues, with the exception of liver that was normalized to *Hsp90* and *Gusb*. For measuring L1 transcription, poly(A) RNA samples were exhaustively digested with RNase-free DNase (Qiagen) before the synthesis of cDNA[6]. Effectiveness of the DNase digestion was assessed using controls that omitted the RT enzyme.

Design of PCR primers. Primer sets 1 to 5 (Supplementary Table 1, amplicons A to E in Fig. 1b) to human L1 were designed to preferentially amplify elements of the human-specific L1HS and evolutionarily recent primate-specific L1PA(2–6) subfamilies, as follows. First, the consensus sequences of L1HS and L1PA2 through L1PA6 elements were obtained from Repbase (Genetic Information Research Institute, http://www.girinst.org/repbase/update/browse.php). Second, a consensus sequence of these six sequences was generated with the Clustal Omega multiple sequence alignment tool (http://www.ebi.ac.uk/Tools/msa/clustalo/)[39]. Primer design was then done on the overall consensus with Primer3 and BLAST using the NCBI Primer-BLAST tool (http://www.ncbi.nlm.nih.gov/primer-blast/)[40]. L1 primer pairs were evaluated for their targets using the In-Silico PCR (https://genome.ucsc.edu/cgi-bin/hgPcr) tool against the latest genome assembly (hg38) with a minimum perfect match on 3′ end of each primer equal to 15. Primers to *ORF2* (primer set 6, amplicon F in Fig. 1b) were developed previously[16] to preferentially target L1HS. Primers to assess transcription of active mouse L1 elements (primer set 37, Supplementary Table 1) were designed on the combined consensus sequence of the L1MdA and L1Tf families obtained from Repbase and validated as described above. L1 primer pairs spanning the full length of these elements (primer sets 48–50) were designed using the same strategy. Primer pairs specific to the three active families of mouse L1 elements (primer sets 51–53) were designed exploiting polymorphisms in the 5′ UTR region. RT–qPCR analysis of L1 transcription was performed on poly(A)-purified RNA using the SYBR Green method. For all other (non-L1) genes, whenever possible, primers were separated by at least one intron in the genomic DNA sequence (as indicated in Supplementary Table 1). Primers to the human IFNA family were designed against a consensus sequence of all human IFNA gene sequences (*IFNA1*, *IFNA2*, *IFNA4*, *IFNA5*, *IFNA6*, *IFNA7*, *IFNA8*, *IFNA10*, *IFNA13*, *IFNA14*, *IFNA16*, *IFNA17* and *IFNA21*) generated with the Clustal Omega multiple sequence alignment tool. All primers against mouse targets were designed as described above and are listed in Supplementary Table 1. Sequences of primers corresponding to a consensus of all mouse IFNA family genes, as well as to the *IFNB1* gene, were as described previously[41]. To quantify relative L1 genomic copy number (human cells) we used the TaqMan multiplex method developed previously[16]. These primers are listed as set #6 and set #7 (with their corresponding VIC and 6FAM probes) in Supplementary Table 1.

Chromatin immunoprecipitation. All ChIP experiments were performed using the Chromatrap spin column ChIP kit (Porvair). In brief, 2×10^6 cells were crosslinked in their culture dishes with 1% formaldehyde (10 min, room temperature), quenched with glycine, washed twice with ice-cold PBS (containing protease inhibitors), and finally scraped into a microfuge tube. Cell pellets were resuspended in 0.4 ml of hypotonic buffer and incubated for 10 min on ice. Nuclei were spun down, resuspended in 0.3 ml lysis buffer, and sonicated using a Bioruptor UCD-200 instrument (Diagenode) set to pulse on high (30 s, followed by 30 s rest) for a total time of 10 min. The extracts were centrifuged in a microfuge (top speed, 5 min, 4 °C) to remove debris, the supernatants were transferred to new tubes, and stored at −80 °C. An amount of extract containing 2 μg of DNA was combined with 4 μg of antibody and loaded on a Chromatrap solid phase Protein A matrix.

Immunocomplexes were allowed to form overnight at 4 °C with mild agitation, following which the samples were washed and eluted according to the manufacturer's protocol. Rabbit IgG and 1% input were used as controls. One microlitre of immunoprecipitated DNA was used in each qPCR reaction.

BrdU pull-down. To obtain quiescent cells, proliferating cells were grown to 50% confluence, serum supplementation of the medium was changed to 0.1% FBS, and incubation was continued until collection. Quiescent and senescent cells were continuously labelled for two weeks with BrdU (BrdU Labelling Reagent, Thermo Fisher) according to the manufacturer's protocol for labelling of culture cells. Cell were collected and counted; 5×10^5 cells were processed per condition. Genomic DNA was purified via phenol–chloroform extraction, RNase A-treated, and subsequently sheared using a Bioruptor UCD-200 instrument (pulse on low, 30 s on and 30 s off, 10 min total). DNA tubes were incubated in a heat block (100 °C) for exactly 1 min and then flash-frozen in liquid nitrogen. Tubes were let thaw at room temperature and 1 μg of purified anti-BrdU antibody (BD Pharmingen, 555627) was added per tube together with magnetic protein A/G beads and ChIP dilution buffer. Immuno-slurries were incubated overnight at 4 °C with constant rotation. Immuno-captured BrdU labelled DNA was purified according to the Magna ChIP A/G Chromatin Immunoprecipitation Kit (Millipore, Sigma). Unbound DNA was kept as input. One microlitre of immunoprecipitated DNA was used in each qPCR reaction. Alternatively, to enrich for single-stranded BrdU-labelled DNA the heat-mediated denaturation was omitted and samples were processed for BrdU pull-down as above. The DNA second-strand was then generated by adding a mixture of random primers (Thermo Fisher), second-strand synthesis reaction buffer, dNTPs and DNA Pol I (New England Biolabs). The reaction was incubated for 4 h at 16°C and subsequently purified by phenol–chloroform extraction. Following the second-strand synthesis, the double-stranded DNA was end-repaired with the End-It DNA End-Repair Kit (Epicentre, ER0720). Blunt-ended fragments were cloned using the Zero Blunt TOPO PCR Cloning Kit (Thermo Fisher), and then used to transform One Shot TOP10 chemically competent *Escherichia coli* (Thermo Fisher, C404010). Individual colonies were picked and subjected to Sanger sequencing using a T7 promoter primer at Beckman Coulter Genomics.

RNA-seq. Total RNA from early passage, early and deep senescent cells (Extended Data Fig. 1a) was extracted as described above. The total RNA was processed with the Illumina TruSeq Stranded Total RNA Ribo-Zero kit and subjected to Illumina HiSeq2500 2 ×125-bp paired-end sequencing using v4 chemistry at Beckman Coulter Genomics Inc. More than 70 million reads were obtained for each sample. The RNA-seq experiment was performed in three biological replicates.

Raw RNA-seq reads were aligned to the GrCh38 build of the human genome using HiSat2[42]. Counts mapping to the genome were determined using featureCounts[43]. Counts were then normalized using the trimmed mean of M-values (TMM) method in EdgeR[44]. EdgeR was additionally used to derive differential expression from the normalized dataset. Differential expression data were then ranked by $\log_2$ fold change and input into the GenePattern interface for GSEA Preranked, using 1,000 permutations, to determine enrichment for KEGG pathways, SASP, and the interferon response[45,46]. The outputs were then corrected for multiple comparisons by adjusting the nominal *P* value using the Benjamini–Hochberg method[47]. Data were displayed using GENE-E software (http://www.broadinstitute.org/cancer/software/GENE-E).

In silico analysis of transcription factors binding to L1. Transcription factor profiles were created using ChIP–seq data from the ENCODE project (GEO accession numbers GSE2961 and GSE32465). Transcription factor ChIP–seq and input control reads were aligned to the consensus sequence of L1HS using bowtie1[48]. The fold change, $\log_2$(enrichment), was calculated per base pair of the L1HS consensus using the transcription factor ChIP–seq read coverage per million mapping reads (RPM) versus input control RPM values, and smoothed by LOESS smoothing with a parameter $\alpha = 0.1$. The total number of mapping reads used in RPM normalization was determined from a separate bowtie1 alignment to the human genome (hg19).

Construction of FOXA1 reporters. L1 promoter reporter plasmids L1WT and L1del (390–526) were obtained from S. Dmitriev[49,50]. Both contain luciferase as the reporter cloned in the sense orientation. To determine antisense transcription from the same plasmid EYFP was inserted in the inverse orientation upstream of the L1 5′ UTR as follows. The EYFP sequence was excised from pEYFP-N1 (Clontech, 6006-1) with AgeI and NotI and blunt ended. Plasmids L1WT and L1del were digested with XbaI, blunted and treated with FastAP (Fermentas). Successful insertion of anti-sense EYFP was verified using PCR primers AAAGTTTCTTATGGCCGGGC (in EYFP) and GCTGAACTTGTGGCCGTTTA (in L1 promoter) and Sanger sequencing. Plasmid pcDNA3.1/LacZ was used as the co-transfection control. Luciferase and β-galactosidase assays were performed as described[49]. EYFP-N1 was used as a positive control for detecting the EYFP signal. Co-transfections were performed on early passage LF1 cells using Lipofectamine with Plus Reagent (Invitrogen) according to the manufacturer's instructions.

Lentiviral vectors. Constructs were obtained from public depositories as indicated below. Virions were produced and target cells were infected as described (https://www.addgene.org/tools/protocols/plko/). shRNA sequences were obtained from The RNAi Consortium (TRC, http://www.broad.mit.edu/genome_bio/trc/rnai.html), cloned into third-generation pLKO.1 vectors and tested for efficacy. Four selectable markers were used to allow multiple drug selections: pLKO.1 puro (2 μg ml^{-1}) and pLKO.1 hygro (200 μg ml^{-1}) (gifts from B. Weinberg, Addgene plasmid 8453, 24150), pLKO.1 blast (5 μg ml^{-1}) (gift from K. Mostov, Addgene plasmid 26655), and pLKO.1 neo (250 μg ml^{-1}) (gift from S. Stewart, Addgene plasmid 13425). pLKO-RB1-shRNA63 and pLKO-RB1-shRNA19 were gifts from T. Waldman (Addgene plasmids 25641 and 25640)[51]. For *FOXA1* shRNAs, TRCN0000014881 (a) and TRCN0000014882 (b) were used. For *TREX1* shRNAs, TRCN0000007902 (a) and TRCN0000011206 (b) were used. For knockdown of L1, we designed and tested nine shRNAs, of which two (shL1_11 to ORF1, AAGCAGTGTGTAGAGGGAAAT, and shL1_44 to ORF2, AAGACACATGCACACGTATGT) showed significant knockdown (Extended Data Fig. 5g) and were chosen for further work. The remaining seven shRNAs produced no or minimal knockdown. For *CGAS* shRNAs, TRCN0000128706 (a) and TRCN0000128310 (b) were used. For *STING* shRNAs, TRCN0000161345 (a) and TRCN0000135555 (b) were used.

All ectopic expression experiments used constructs generated by the ORFeome Collaboration (http://www.orfeomecollaboration.org/) in the lentivirus vector pLX304 (blasticidin resistant, Addgene plasmid 25890) and were obtained from the DNASU plasmid repository (https://dnasu.org/DNASU/Home.do): RB1 (ccsbBroad304_06846, HsCD00434323), TREX1 (ccsbBroad304_02667, HsCD00445909), FOXA1 (ccsbBroad304_06385, HsCD00441689).

All the interventions in senescent cells were initiated by infecting cells at 12 weeks of senescence (point D in Extended Data Fig. 1a). After appropriate drug selections, cells were incubated until 16 weeks of senescence (point E in Extended Data Fig. 1a), when they were collected for further analysis.

The 3× intervention was performed by infecting early passage LF1 cells sequentially with vectors pLKO.1 puro shRB, pLKO.1 hygro shTREX1 and pLX304 blast FOXA1 (Extended Data Fig. 5c). After each infection, the arising drug-resistant pool of cells was immediately infected with the next vector. After the third infection, the cells were collected for further analysis 48 h after the drug selection was complete. The infections were also performed in various combinations and in each case resulted in the activation of L1 expression, entry into senescence, and induction of an IFN-I response. The sequence above was chosen because it gave the most efficient selection of cells for further analysis. To allow an additional (fourth) intervention in 3× cells (shL1, shSTING or shCGAS), shRNAs targeting *RB1* were recloned in pLKO.1 neo, thus freeing pLKO.1 puro for the fourth gene of interest. This allowed an efficient drug selection process and sample harvest 48 h after the last selection.

Retrotransposition reporters. The two-vector dual luciferase reporter system reported previously[52] was adapted for lentiviral delivery. The $L1_{RP}$-FLuc reporters were recloned from plasmids pWA355 and pWA366 into the lentiviral backbone pLX304. pWA355 contains a functional, active $L1_{RP}$ element, whereas pWA366 contains $L1_{RP}$(JM111), a mutated element carrying two missense mutations in ORF1 that is unable to retrotranspose. Early passage LF1 cells were infected with a puromycin-resistant lentivirus expressing RLuc. Pooled drug-resistant cells were then infected with high-titre particles of pLX304-WA355 or pLX304-WA366 constructs. Immediately after infection, cells were treated for four days with 3TC (at the indicated concentrations). Cells were then collected and assayed for RLuc and FLuc luciferase activities. The native L1 retrotransposition reporter pLD143[53] was co-transfected with pLKO vectors (shLuc, shL1_11 and shL1_44) into HeLa cells using FuGene HD (Promega). Cell culture, transfection and retrotransposition assays were done as described above. Retrotransposition activity was normalized to the activity of $L1_{RP}$ co-transfected with shLuc. Three independent experiments were performed for each construct.

Identification of expressed L1 elements by long-range RT–PCR and 5′ RACE. Total RNA was collected from cells using the Trizol reagent (Invitrogen). The RNA was further purified using the Purelink RNA Mini kit (Invitrogen) with DNase I digestion. From the eluted total RNA, poly(A) RNA was isolated using the NEBNext Poly(A) mRNA Magnetic Isolation Module (New England Biolabs). The forward primer (MDL15UTRPRAF, primer set 1, Supplementary Table 1) was used with either of two reverse primers (MDL15UTRPRCR, primer set 3, amplicon size 537 bp) or MDL15UTRPRDR, primer set 4, amplicon size 654 bp). A high-fidelity thermostable reverse transcriptase (PyroScript RT–PCR Master Mix Kit, Lucigen) was used with 10 ng of poly(A) mRNA per reaction and amplified for 10 cycles. No template and RNaseA treated samples were used as negative controls. The generated amplicons were cloned into the TOPO-TA (Invitrogen) vector and the resulting plasmids were used to transform One Shot TOP10 chemically competent *E. coli*. Individual colonies were picked and subjected to Sanger sequencing using a T7 promoter sequencing primer at Beckman Coulter Genomics. A total

of 96 sequencing reactions (1 plate) were performed for each primer pair in four experiments for a total of 768 sequenced clones. Sequencing data were trimmed to remove the RT–PCR primers and BLASTed against the human genome (GRCh38) with a match/mismatch cost of +1, −4 and allowing species-specific repeats for *Homo sapiens*. Only perfect hits were scored and annotated for genomic coordinates. 658 clones could be mapped to the reference genome, 51 contained at least 1 mismatch and thus likely represent elements that are polymorphic in the cell line, and 58 were cloning artefacts. Whenever a clone presented multiple instances of perfect identity a fractional count was adopted, dividing the counts by the number of elements sharing the same sequence. Each mappable clone was further analysed using L1Xplorer[54] to recover the classification features of the L1 element and determine whether it is intact.

Alternatively, poly(A) RNA isolated as above was subjected to RACE. Each reaction contained 10 ng of poly(A) RNA and was processed using the 5′RACE System kit (Thermo Fisher, 18374-041). The two antisense gene-specific primers (GSP) used for 5′RACE were: for GSP1, MDL15UTRPRDR (primer set 4, Supplementary Table 1), and for the nested GSP2, MDL15UTRPRCR (primer set 3, Supplementary Table 1). Amplification products were cloned and sequenced as above, using a T7 promoter sequencing primer by Beckman Coulter Genomics. A total of 94 clones were sequenced; 26 contained mostly a polyG stretch generated by the tailing step in the RACE protocol and 18 could not be mapped to the human genome. The remaining 50 mappable clones contained L1 sequences and were aligned to the L1HS consensus using a setting of >95% identity at positions 1–450 (http://www.girinst.org/repbase/update/browse.php). The mappable clones were also assigned to individual L1 families using RepEnrich software[55]. Pairwise alignments to the consensus were performed with LALIGN[56]. Multiple sequence alignments were calculated using MAFFT (Multiple Alignment using Fast Fourier Transform) with the L-INS-i algorithm (accurate for alignments of <200 sequences)[57]. Alignment visualization, percentage identity colouring and consensus were generated by Jalview[58].

Generation and analysis of CRISPR–Cas9 knockouts. Three distinct guide RNA (gRNA) sequences for each chain of the IFNA receptor (*IFNAR1* and *IFNAR2*), listed in the GeCKO v2.0 resource (F. Zhang laboratory, MIT, http://genome-engineering.org/gecko/?page_id=15)[59], were tested and the following ones were chosen: *IFNAR1* (HGLibA_29983) AACAGGAGCGATGAGTCTGTA; *IFNAR2* (HGLibA_29985) GTGTATATCAGCCTCGTGTT. Cas9 and gRNAs were delivered using a single lentivirus vector (LentiCRISPR_v2, Feng Zhang Laboratory, MIT; Addgene plasmid 52961), carrying a puromycin-resistance gene. The efficacy of the CRISPR–Cas9 mutagenesis, on the basis of which the above two gRNAs were chosen, was evaluated by treating the infected and drug-selected cells with interferon (universal type I interferon, PBL Assay Science, 11200-1) and monitoring nuclear translocation of phospho-STAT2 and IRF9 by immunofluorescence. The absence of translocation signifies lack of IFN-I responsiveness and hence loss of IFNAR function. Experimental procedures followed the protocols provided by the Zhang laboratory (https://benchling.com/protocols/cNzMcO/cloning-customsgrnas-into-crispr-lentiviral-vectors)[60]. In the experiments shown in Fig. 3d (replicative senescence) and Extended Data Fig. 5m, both *IFNAR1* and *IFNAR2* gRNAs were used to treat the same cells to further increase the efficacy of ablating the INF-I response. For early passage and senescent cells, co-infections of IFNAR1 and IFNAR2 vectors were performed followed by selection with puromycin. For senescent cells, high-titre lentivirus particles were applied to senescent cells at 12 weeks in senescence (point D, Extended Data Fig. 1a) and cells were assayed 4 weeks later (point E, Extended Data Fig. 1a). For the experiment shown in Fig. 3d (SIPS), edited early passage cells were single-cell cloned. 24 single cells were isolated using the CellRaft technology (Cell Microsystems) and expanded. Genomic screening of the CRISPR cut site was performed by the CRISPR Sequencing Service (CCIB DNA Core, Massachusetts General Hospital, https://dnacore.mgh.harvard.edu/). The successful knockout of IFNAR1 and IFNAR2 was verified in 4 out of the 24 expanded clonal cell lines.

Immunoblotting. Cells were collected in Laemmli sample buffer (60 mM Tris pH 6.8, 2% SDS, 10% glycerol, 100 mM DTT) and boiled for 5 min at 100°C. Whole-cell extracts (60 μg protein) were separated by SDS–PAGE and transferred onto Immobilon-FL membranes (Millipore). Non-specific binding was blocked by incubation in 4% bovine serum albumin (BSA; Thermo Fisher) and 0.1% Tween-20 in PBS for 1 h at room temperature. Primary antibodies were diluted in the blocking solution and incubated overnight at 4 °C. A list of all the primary antibodies is provided in Supplementary Table 2. Secondary antibodies were diluted in blocking solution and incubated for 1 h at room temperature. Signals were detected using the LI-COR Odyssey infrared imaging system (LI-COR Biosciences). For the quantification of signals, all samples to be compared were run on the same gel. Loading standards were visualized on the same blot as the test samples using the LI-COR 2-colour system. Bands were imaged and quantified using LI-COR software. All bands to be compared were quantified on the same image and were within the linear range of detection of the instrument.

Immunofluorescence microscopy performed on cells in culture. Cells were grown on glass cover slips and the samples were processed as previously described[61]. Primary antibodies are listed in Supplementary Table 2. Staining of ssDNA was performed as described previously[11]. In brief, cells seeded on coverslips were fixed on ice with 4% paraformaldehyde (PFA) for 20 min and then incubated in 100% methanol at −20 °C overnight. The cells were then treated with 200 mg ml^{-1} RNase A at 37 °C for 4 h. Cells were blocked with 3% BSA and incubated overnight at 4 °C with primary antibodies diluted in 3% BSA. Images were acquired using a Zeiss LSM 710 confocal laser scanning microscope or a Nikon Ti-S inverted fluorescence microscope. All microscope settings were set to collect images below saturation and were kept constant for all images taken in one experiment, as previously described[61]. Image analysis was performed as described below for tissues.

PCR arrays. Total RNA was collected from cells as indicated above (see 'PCR' section) and analysed using the Qiagen RT^2 Profiler Human Type I Interferon Response PCR Array (PAHS-016ZE-4). Reverse transcription reactions were performed with the Qiagen RT^2 First Strand Kit (330404) using 1 μg of total RNA as starting material. Then, 102 μl of the completed reaction was combined with 650 μl of Qiagen RT^2 SYBR Green ROX qPCR Mastermix (330521) and 548 μl of RNase-free molecular grade water, and run in the 384-well block on a ViiA 7 Applied Biosystems instrument. All procedures followed the manufacturer's protocols. All conditions were run in triplicate. The results were analysed using the Qiagen GeneGlobe Data Analysis Center (http://www.qiagen.com/us/shop/genes-and-pathways/data-analysis-center-overview-page/). In brief, C_t values were normalized to a panel of housekeeping genes. ΔC_t values were calculated between a gene of interest and the mean housekeeping genes value. Fold changes were then calculated using $2^{-\Delta\Delta Ct}$ formula. The lower limit of detection was set at C_t of 35. For any gene of interest to be considered significant, the following filters were set: (1) more than twofold change in expression; and (2) $P > 0.05$. In addition, genes with an average $C_t > 32$ in both control and test samples were also eliminated.

ELISA. IFNβ levels were quantified with the VeriKine-HS Human IFN Beta Serum ELISA Kit (PBL Assay Science, 41415). Cell culture media were conditioned for 48 h before collection. To remove particles and debris, 1-ml aliquots were spun for 5 min at 5,000*g*. All incubations were performed in a closed chamber at room temperature (22–25 °C) keeping the plate away from temperature fluctuations. Next, 50 μl of sample buffer followed by 50 μl of diluted antibody solution were added to each well. Finally, 50 μl of test samples, standards or blanks were added per well. Plates were sealed and shaken at 450 r.p.m. for 2 h. At the end of the incubation period, the contents of the plate were removed and the wells were washed three times with 300 μl of diluted wash solution. Horseradish peroxidase (HRP) solution (100 μl) was added to each well and incubated for 30 min under constant shaking. The wells were emptied and washed four times with wash solution. TMB substrate solution (100 μl) was added to each well. Plates were incubated in the dark for 30 min. Finally, 100 μl of stop solution was added to each well and within 5 min absorbance at 450 nm was recorded. The values recorded for the blank controls were subtracted from the standards as well as sample values to eliminate background. Optical density (OD) units were plotted using a 4-parameter fit for the standard curve and were used to calculate the interferon titres in the samples.

Human tissue specimens. Human skin specimens were collected as part of the Leiden Longevity Study[62,63] and were provided by P.E.S. Informed consent was obtained and all protocols were approved by the ethical committee of the Leiden University Medical Centre. The samples were collected as 4-mm thickness full-depth punch biopsies, embedded in optimal cutting compound (OCT), flash-frozen, and stored at −80 °C. Samples were shipped on dry ice to Brown University. The Brown investigators were blinded to everything except the age and sex of the subjects. The OCT-embedded specimens were cryosectioned at 8-μm thickness using a Leica CM3050S cryomicrotome. The slides were fixed with 4% PFA and 0.5% Triton X-100 in PBS (pre-warmed to 37 °C) for 20 min at room temperature. No further permeabilization was performed. Antibody incubation was preceded by a blocking step with 4% BSA (fraction V, Thermo Fisher), 2% donkey serum, 2% rabbit serum and 0.1% Triton X-100 in PBS for 1 h at room temperature. Primary antibodies were diluted in the above blocking solution (1:200) and incubated overnight at 4 °C with rocking in a humidified chamber. The secondary antibodies (AlexaFluor 546 and AlexaFluor 647, Life Technologies) were also diluted in blocking solution and incubated for 2 h at room temperature. Three 15-min washing steps in PBS, containing 0.2% Triton X-100, followed each antibody incubation. Nuclei were counterstained with 2 μg ml^{-1} DAPI in PBS, containing 0.2% Triton X-100, for 15 min. Stained slides were mounted with ProLong Antifade Mountant without DAPI (Life Technologies) and imaged on a Zeiss LSM 710 Confocal Laser Scanning Microscope. A *z*-series encompassing the full thickness of the tissue was collected for each field. All microscope settings and exposure times were set to collect images below saturation and were kept constant for all images taken in one experiment. Image analysis was performed using either CellProfiler software[64], or ImageJ open source software from the NIH (http://rsbweb.nih.gov/ij/).

Nuclei were defined using the DAPI channel. Cell outlines were defined by radially expanding the nuclear mask using the function 'Propagate' until an intensity threshold in the AlexaFluor 546 and AlexaFluor 647 channels was reached. The fluorescence intensity within these regions was then recorded in both channels. A total of 200 cells in several fields were scored for each condition. Mouse tissue sections were processed and analysed in the same way as described above.

Mouse tissue specimens. Total RNA was extracted from 50 mg of visceral adipose, small intestine, skeletal muscle, brown adipose or liver tissue by mincing followed by homogenization in Trizol (Invitrogen) using a Power Gen 125 homogenizer (Fischer Scientific). After phase separation, the RNA in the aqueous layer was purified using the Purelink RNA Mini kit (Invitrogen) with DNase I digestion. To assess gene expression by RT–qPCR 1 μg of total RNA was reverse transcribed as described above. In each individual experiment all samples were processed in parallel and no blinding was introduced.

Imaging of whole-mount white adipose tissue followed the method described previously[65]. In brief, white adipose tissue (visceral depot) was subdivided into 0.5–1.0 cm^3 sized pieces and incubated in 10 ml of fresh fixing buffer (1% PFA in PBS pH 7.4) for 30 min at room temperature with gentle rocking. After three washing steps with PBS, the tissue blocks were cut into six equal pieces. All subsequent incubations were performed in 2-ml cylindrical microcentrifuge tubes. Primary antibody incubation was preceded by a blocking step with 5% BSA and 0.1% saponin in PBS for 30 min at room temperature. Primary antibodies were diluted in the above blocking solution (1:200) and incubated overnight at 4 °C with gentle rocking. The secondary antibodies (AlexaFluor 546, AlexaFluor 594 and AlexaFluor 647, Life Technologies) were also diluted in blocking solution and incubated for 2 h at room temperature. Three 10-min washing steps in PBS followed each antibody incubation. Antibody-independent staining of nuclei and lipids was performed after immunostaining: DAPI and BODIPY (Thermo Fisher) were diluted in PBS with 5% BSA and incubated with tissue specimens for 20 min followed by three washing steps as above. Stained samples were carefully placed on confocal-imaging-optimized #1.5 borosilicate glass chamber slides. A small drop of PBS prevented drying. Acquired images were analysed as described above.

Co-staining of SA-β-Gal activity and ORF1 protein in liver sections was performed by staining for SA-β-Gal first as described[66]. Subsequently, samples underwent heat-induced epitope retrieval by steaming for 20 min in antigen retrieval buffer (10 mM Tris, 1 mM EDTA, 0.05% Tween 20, pH 9.0). Samples were then processed for immunofluorescence staining as described in the 'Human tissue specimens' section.

Kidney tissue preserved in OCT was cryosectioned, treated for 10 min with 0.5% (w/v) periodic acid, then stained with periodic acid-Schiff's (PAS) reagent (Fisher Scientific, SS32-500) for 10 min. Stained tissue sections were mounted with Shandon Aqua Mount (Fisher Scientific, 14-390-5) and then imaged under bright-field illumination. Glomerulosclerosis was scored as described[26]. In brief, 40 glomeruli per animal were assessed in a blinded fashion and assigned scores of 1–4: score of 1, <25% sclerosis; 2, 25–50% sclerosis; 3, 50–75% sclerosis; 4, >75% sclerosis. The feature used to assess sclerosis was the strength and pervasiveness of PAS-positive lesions within the glomeruli. As exemplified in Fig. 4e, a sclerotic glomerulus is more shrunken and stains more intensely with PAS.

Quadriceps muscles were embedded in OCT, sectioned at 12-μm thickness and mounted onto positively charged slides. Sections were stained with haematoxylin and eosin (H&E; (haematoxylin for 3 min, followed by 30 s in eosin). Mounted slides were imaged on a Zeiss Axiovert 200M microscope equipped with a Zeiss MRC5 colour camera. To measure muscle fibre diameter, the shortest distance across approximately 100 muscle fibres per animal was measured using ImageJ software as described[27].

Statistical treatments. Excel was used to perform general statistical analyses (such as mean, s.d. and *t*-tests). R software for statistical computing (64-bit version 3.3.2) was used for one-way ANOVA and Tukey's multiple comparisons post hoc test. For consistency of comparisons, significance in all figures is denoted as follows: $*P < 0.05$, $**P < 0.01$. Sample sizes were based on previously published experiments and previous experience in which differences were observed. No statistical test was used to pre-determine sample size. No samples were excluded. All attempts at replication were successful. There were no findings that were not replicated or could not be reproduced. The nature and numbers of samples analysed (defined as *n*) in each experiment are listed in the figure legends. The number of independent experiments is also listed. The investigators were blinded when quantifying immunofluorescence results. Fields or sections of tissues for quantification were randomly selected and then scored, using methods as indicated for individual experiments. The investigators were also blinded when scoring glomerulosclerosis and muscle fibre diameter. For RNA-seq and PCR array experiments, the statistical treatments are described under those sections.

Reporting summary. Further information on research design is available in the Nature Research Reporting Summary linked to this paper.

Data availability

All Source Data and exact *P* values (if applicable) for every figure are included in the supporting information that accompanies the paper. RNA-seq data have been deposited in the Gene Expression Omnibus (GEO) with accession number GSE109700. Any other data or information relevant to this study are available from the corresponding author upon reasonable request.

33. Brown, J. P., Wei, W. & Sedivy, J. M. Bypass of senescence after disruption of $p21^{CIP1/WAF1}$ gene in normal diploid human fibroblasts. *Science* **277**, 831–834 (1997).
34. Herbig, U., Jobling, W. A., Chen, B. P., Chen, D. J. & Sedivy, J. M. Telomere shortening triggers senescence of human cells through a pathway involving ATM, p53, and $p21^{CIP1}$, but not $p16^{INK4a}$. *Mol. Cell* **14**, 501–513 (2004).
35. Fumagalli, M., Rossiello, F., Mondello, C. & d'Adda di Fagagna, F. Stable cellular senescence is associated with persistent DDR activation. *PLoS One* **9**, e110969 (2014).
36. Ambati, J., Fowler, B. & Ambati, K. Compositions and methods for treating retinal degradation. US patent WO/2016/138425 (2016).
37. Else, L. J. et al. Pharmacokinetics of lamivudine and lamivudine-triphosphate after administration of 300 milligrams and 150 milligrams once daily to healthy volunteers: results of the ENCORE 2 study. *Antimicrob. Agents Chemother.* **56**, 1427–1433 (2012).
38. Le, O. N. et al. Ionizing radiation-induced long-term expression of senescence markers in mice is independent of p53 and immune status. *Aging Cell* **9**, 398–409 (2010).
39. Li, W. et al. The EMBL-EBI bioinformatics web and programmatic tools framework. *Nucleic Acids Res.* **43** (W1), W580–W584 (2015).
40. Ye, J. et al. Primer-BLAST: a tool to design target-specific primers for polymerase chain reaction. *BMC Bioinformatics* **13**, 134 (2012).
41. Gautier, G. et al. A type I interferon autocrine-paracrine loop is involved in Toll-like receptor-induced interleukin-12p70 secretion by dendritic cells. *J. Exp. Med.* **201**, 1435–1446 (2005).
42. Kim, D., Langmead, B. & Salzberg, S. L. HISAT: a fast spliced aligner with low memory requirements. *Nat. Methods* **12**, 357–360 (2015).
43. Liao, Y., Smyth, G. K. & Shi, W. featureCounts: an efficient general purpose program for assigning sequence reads to genomic features. *Bioinformatics* **30**, 923–930 (2014).
44. Robinson, M. D., McCarthy, D. J. & Smyth, G. K. edgeR: a Bioconductor package for differential expression analysis of digital gene expression data. *Bioinformatics* **26**, 139–140 (2010).
45. Reich, M. et al. GenePattern 2.0. *Nat. Genet.* **38**, 500–501 (2006).
46. Subramanian, A. et al. Gene set enrichment analysis: a knowledge-based approach for interpreting genome-wide expression profiles. *Proc. Natl Acad. Sci. USA* **102**, 15545–15550 (2005).
47. Benjamini, Y. & Hochberg, Y. Controlling the false discovery rate: a practical and powerful approach to multiple testing. *J. R. Stat. Soc. B* **57**, 289–300 (1995).
48. Langmead, B. Aligning short sequencing reads with Bowtie. *Curr. Protoc. Bioinformatics* Chapter 11, Unit 11.7 (2010).
49. Alexandrova, E. A. et al. Sense transcripts originated from an internal part of the human retrotransposon LINE-1 5′ UTR. *Gene* **511**, 46–53 (2012).
50. Olovnikov, I. A. et al. A key role of the internal region of the 5′-untranslated region in the human L1 retrotransposon transcription activity. *Mol. Biol. (Mosk.)* **41**, 508–514 (2007).
51. Michaud, K. et al. Pharmacologic inhibition of cyclin-dependent kinases 4 and 6 arrests the growth of glioblastoma multiforme intracranial xenografts. *Cancer Res.* **70**, 3228–3238 (2010).
52. Xie, Y., Rosser, J. M., Thompson, T. L., Boeke, J. D. & An, W. Characterization of L1 retrotransposition with high-throughput dual-luciferase assays. *Nucleic Acids Res.* **39**, e16 (2011).
53. An, W. et al. Characterization of a synthetic human LINE-1 retrotransposon ORFeus-Hs. *Mob. DNA* **2**, 2 (2011).
54. Penzkofer, T., Dandekar, T. & Zemojtel, T. L1Base: from functional annotation to prediction of active LINE-1 elements. *Nucleic Acids Res.* **33**, D498–D500 (2005).
55. Criscione, S. W., Zhang, Y., Thompson, W., Sedivy, J. M. & Neretti, N. Transcriptional landscape of repetitive elements in normal and cancer human cells. *BMC Genomics* **15**, 583 (2014).
56. Childs, B. G., Durik, M., Baker, D. J. & van Deursen, J. M. Cellular senescence in aging and age-related disease: from mechanisms to therapy. *Nat. Med.* **21**, 1424–1435 (2015).
57. Katoh, K. & Standley, D. M. MAFFT multiple sequence alignment software version 7: improvements in performance and usability. *Mol. Biol. Evol.* **30**, 772–780 (2013).
58. Waterhouse, A. M., Procter, J. B., Martin, D. M., Clamp, M. & Barton, G. J. Jalview Version 2-a multiple sequence alignment editor and analysis workbench. *Bioinformatics* **25**, 1189–1191 (2009).
59. Sanjana, N. E., Shalem, O. & Zhang, F. Improved vectors and genome-wide libraries for CRISPR screening. *Nat. Methods* **11**, 783–784 (2014).
60. Shalem, O. et al. Genome-scale CRISPR-Cas9 knockout screening in human cells. *Science* **343**, 84–87 (2014).
61. Kreiling, J. A. et al. Age-associated increase in heterochromatic marks in murine and primate tissues. *Aging Cell* **10**, 292–304 (2011).
62. Schoenmaker, M. et al. Evidence of genetic enrichment for exceptional survival using a family approach: the Leiden Longevity Study. *Eur. J. Hum. Genet.* **14**, 79–84 (2006).
63. Waaijer, M. E. et al. The number of p16INK4a positive cells in human skin reflects biological age. *Aging Cell* **11**, 722–725 (2012).

64. Kamentsky, L. et al. Improved structure, function and compatibility for CellProfiler: modular high-throughput image analysis software. *Bioinformatics* **27**, 1179–1180 (2011).
65. Martinez-Santibañez, G., Cho, K. W. & Lumeng, C. N. Imaging white adipose tissue with confocal microscopy. *Methods Enzymol*. **537**, 17–30 (2014).
66. Itahana, K., Campisi, J. & Dimri, G. P. Methods to detect biomarkers of cellular senescence: the senescence-associated β-galactosidase assay. *Methods Mol. Biol*. **371**, 21–31 (2007).
67. Schorl, C. & Sedivy, J. M. Analysis of cell cycle phases and progression in cultured mammalian cells. *Methods* **41**, 143–150 (2007).
68. Rangwala, S. H., Zhang, L. & Kazazian, H. H., Jr. Many LINE1 elements contribute to the transcriptome of human somatic cells. *Genome Biol*. **10**, R100 (2009).
69. Athanikar, J. N., Badge, R. M. & Moran, J. V. A. A YY1-binding site is required for accurate human LINE-1 transcription initiation. *Nucleic Acids Res*. **32**, 3846–3855 (2004).

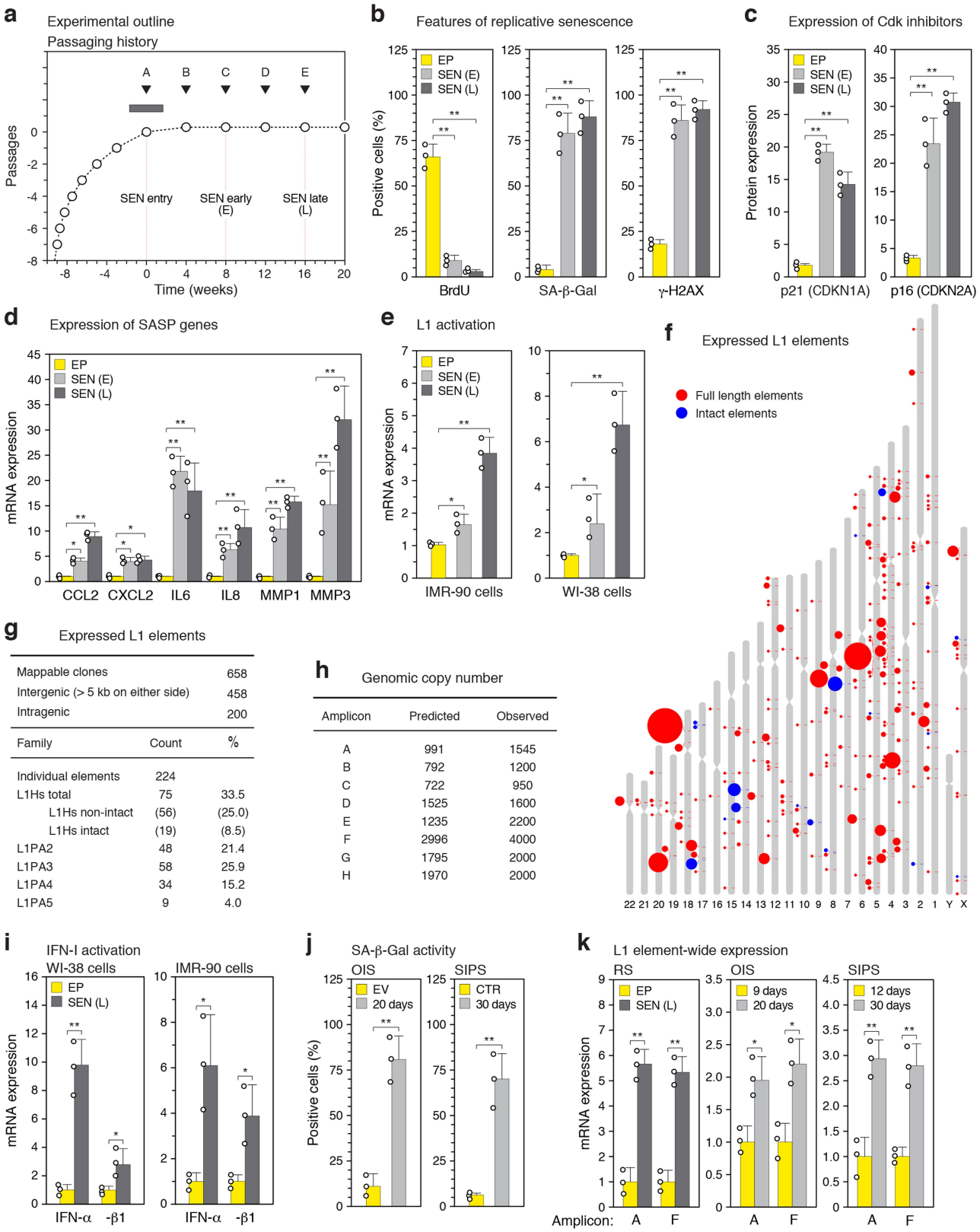

Mappable clones		658
Intergenic (> 5 kb on either side)		458
Intragenic		200
Family	**Count**	**%**
Individual elements	224	
L1Hs total	75	33.5
L1Hs non-intact	(56)	(25.0)
L1Hs intact	(19)	(8.5)
L1PA2	48	21.4
L1PA3	58	25.9
L1PA4	34	15.2
L1PA5	9	4.0

Amplicon	Predicted	Observed
A	991	1545
B	792	1200
C	722	950
D	1525	1600
E	1235	2200
F	2996	4000
G	1795	2000
H	1970	2000

Extended Data Fig. 1 | See next page for caption.

Extended Data Fig. 1 | Establishment of senescent cultures and analysis of L1 and IFN-I activation. a, Passaging regimen to obtain long-term replicatively senescent cells (details in Methods). Point 'A' was designated as zero for time in senescence. **b**–**d**, Confirmation of the senescent status of cultures. A representative experiment is shown; other experiments were monitored in the same manner and generated data that met these benchmarks. **b**, Cells were labelled with BrdU for 6 h. BrdU incorporation[67] and SA-β-Gal activity[66] were determined as indicated. DNA damage foci were visualized using γ-H2AX antibodies and immunofluorescence microscopy[34]. **c**, Expression of p21 (CDKN1A) and p16 (CDKN2A) proteins was determined by immunoblotting. GAPDH was the loading control. For gel source data, see Supplementary Fig. 1. **d**, Expression of genes characteristic of the SASP was determined by RT–qPCR. **e**, L1 activation during senescence of IMR-90 and WI-38 strains of fibroblasts was assessed by RT–qPCR using poly(A)-purified RNA and primers for amplicon F (Fig. 1b). **f**, Long-range RT–PCR was performed with primers A (forward) and C (reverse) (amplicon G) and primers A (forward) and D (reverse) (amplicon H) (Fig. 1b, Supplementary Table 1) and the cDNAs were cloned and sequenced. Several attempts using the same protocol on early passage proliferating cells did not yield any L1 clones. Sequences were mapped to the unmasked reference genome demanding 100% identify. A total of 658 clones could be thus mapped, 51 additional clones contained at least 1 mismatch and thus probably represent elements that are polymorphic in the cell line, and 58 were cloning artefacts. Among the 658 mappable clones, 224 unique elements were represented (Supplementary Table 3). Intact elements are the subset of full-length elements annotated with no ORF-inactivating mutations. Size of the features corresponds to the number of times the element was represented among the 658 clones. **g**, Summary of long-range PCR data presented in **f** and Supplementary Table 3. **h**, Apparent genomic copy numbers of elements detected with our amplicons (see Fig. 1b for locations of amplicons and Methods for primer design strategy). 'Predicted' denotes in silico PCR (Methods); 'observed' denotes qPCR was performed on 1 ng of genomic DNA and normalized to a known single copy locus. **i**, Activation of *IFNA* and *IFNB1* genes during senescence of WI-38 and IMR-90 cells was determined by RT–qPCR. **j**, Confirmation of the senescent status of cells in OIS (20 days, Fig. 1e) and SIPS (30 days, Fig. 1e) by SA-β-Gal activity. **k**, Confirmation of full-length L1 mRNA expression in all forms of senescence using RT–qPCR with primers for amplicons A and F on poly(A)-purified RNA. Late onset activation is shown by comparing days 9 and 20 for OIS, and days 12 and 30 for SIPS. $n = 3$ independent biological samples, repeated in two independent experiments (**b**–**e**, **i**–**k**). Data are mean ± s.d. $*P \leq 0.05$, $**P \leq 0.01$, unpaired two-sided *t*-test. Exact *P* values can be found in the accompanying Source Data.

a

Sequence alignments of 5'RACE data

b

Summary of 5'RACE data

Sequenced clones	50
Start: < –40 bp	4
–25 bp to +25 bp	28
+25 bp to +180 bp	6
> +180 bp	12

Family	Count	%
L1HS	8	16
L1PA2	9	18
L1PA3	11	22
L1PA4	7	14
L1PA5	8	18
L1PA7	2	4
L1P1	5	10

Extended Data Fig. 2 | Mapping transcriptional start sites in L1 elements activated during cellular senescence. 5′ RACE was performed with primers C and D (Fig. 1a, Supplementary Table 1) on late senescent cells (16 weeks, point D in Extended Data Fig. 1a), the products were cloned, and individual clones were Sanger sequenced (Methods). **a**, A multiple sequence alignment of the 50 mappable clones against the L1HS consensus was generated with MAFFT software. The L1HS consensus is shown. Blue shading of the aligned clones shows their degree of identity with the consensus. Green vertical line marks the start (position 1) of the L1HS consensus. Red vertical lines mark short gaps (1–4 nucleotides) opened in the L1HS consensus by individual clones. The consensus of the 50 clones is shown at the bottom and was generated with Jalview. The initiation of L1 transcription is known to be imprecise, with most start sites occurring ±50 bp of the consensus start site, and a subset as far down as +180 bp[68]. **b**, Summary of the mapping data and classification of clones to families of L1 elements. The relative start sites were calculated relative to the L1HS consensus start site. RepEnrich software[55] was used to assign the clones to L1 families.

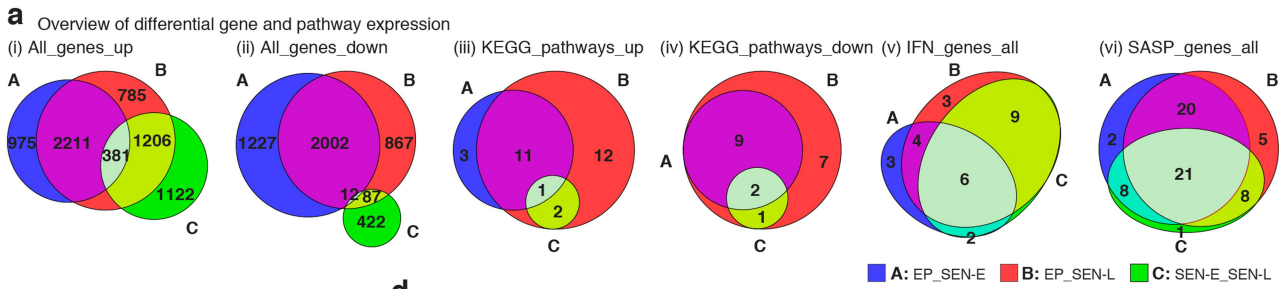

b Summary of significantly regulated genes

	EP_SEN-E		EP_SEN-L		SEN-E_SEN-L	
	UP	DOWN	UP	DOWN	UP	DOWN
2x	3,568	3,241	4,583	2,968	2,708	521
1.75x	4,067	3,824	5,068	3,799	2,948	784
1.5x	4,797	4,620	5,618	4,878	3,200	1,372

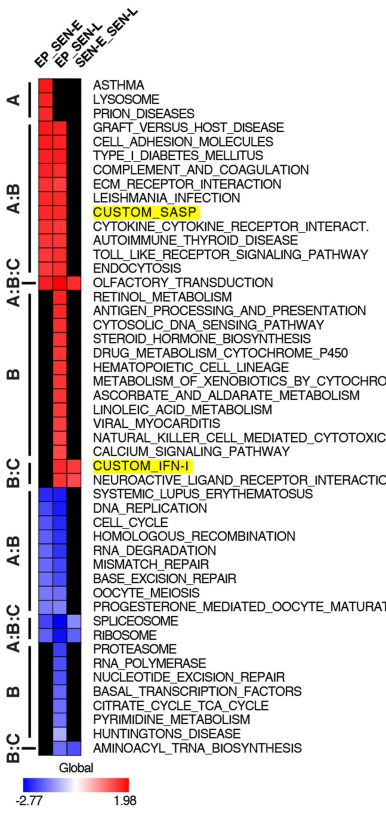

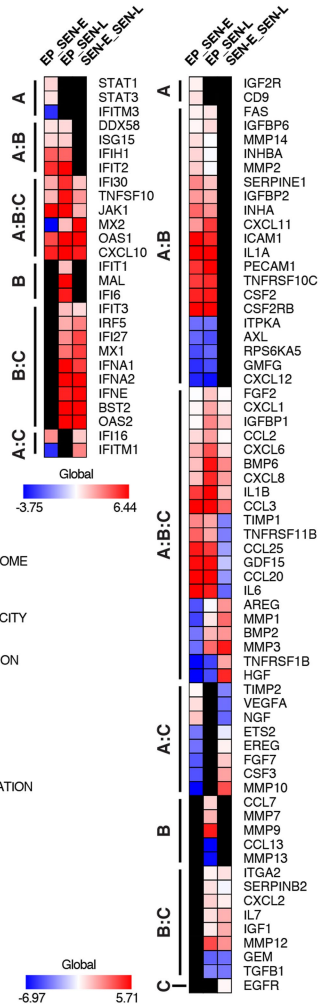

e GSEA analysis of all KEGG pathways

Upregulated from early passage to early senescence (EP_SEN-E_UP)

Pathway name	Size	NES	NOM p-val	FDR p-val
ASTHMA	28	1.7864	<1.00E-03	<1.00E-02
GRAFT_VERSUS_HOST_DISEASE	35	1.7654	<1.00E-03	<1.00E-02
CELL_ADHESION_MOLECULES_CAMS	127	1.7538	<1.00E-03	<1.00E-02
OLFACTORY_TRANSDUCTION	367	1.7468	<1.00E-03	<1.00E-02
TYPE_I_DIABETES_MELLITUS	41	1.7140	<1.00E-03	<1.00E-02
LYSOSOME	119	1.6878	<1.00E-03	<1.00E-02
COMPLEMENT_AND_COAG._CASCADES	67	1.6854	<1.00E-03	<1.00E-02
ECM_RECEPTOR_INTERACTION	84	1.5487	<1.00E-03	<1.00E-02
LEISHMANIA_INFECTION	68	1.6559	1.79E-03	1.51E-02
CUSTOM_SASP	85	1.6517	1.80E-03	1.51E-02
PRION_DISEASES	34	1.6397	1.84E-03	1.51E-02
CYTOKINE_CYTOKINE_RECEPTOR_INTERACT.	254	1.5705	1.62E-03	1.51E-02
TOLL_LIKE_RECEPTOR_SIGNALING_PATHWAY	99	1.4920	1.73E-03	1.51E-02
AUTOIMMUNE_THYROID_DISEASE	48	1.5336	3.77E-03	2.66E-02
ENDOCYTOSIS	174	1.4427	5.21E-03	3.49E-02

Upregulated from early passage to late senescence (EP_SEN-L_UP)

Pathway name	Size	NES	NOM p-val	FDR p-val
OLFACTORY_TRANSDUCTION	367	1.9816	<1.00E-03	<5.00E-03
TYPE_I_DIABETES_MELLITUS	41	1.7551	<1.00E-03	<5.00E-03
GRAFT_VERSUS_HOST_DISEASE	35	1.7098	<1.00E-03	<5.00E-03
CELL_ADHESION_MOLECULES_CAMS	127	1.6868	<1.00E-03	<5.00E-03
RETINOL_METABOLISM	56	1.6689	<1.00E-03	<5.00E-03
CUSTOM_SASP	85	1.6282	<1.00E-03	<5.00E-03
LEISHMANIA_INFECTION	68	1.6260	<1.00E-03	<5.00E-03
CUSTOM_IFN-I	50	1.6248	<1.00E-03	<5.00E-03
COMPLEMENT_AND_COAG._CASCADES	67	1.6008	<1.00E-03	<5.00E-03
TOLL_LIKE_RECEPTOR_SIGNALING_PATHWAY	99	1.5759	<1.00E-03	<5.00E-03
NEUROACTIVE_LIGAND_RECEPTOR_INTERACT.	270	1.5340	<1.00E-03	<5.00E-03
CYTOKINE_CYTOKINE_RECEPTOR_INTERACT.	254	1.5008	<1.00E-03	<5.00E-03
HEMATOPOIETIC_CELL_LINEAGE	85	1.5269	1.07E-03	5.32E-03
DRUG_METABOLISM_CYTOCHROME_P450	63	1.5343	1.12E-03	5.32E-03
ANTIGEN_PROCESSING_AND_PRESENTATION	73	1.6286	1.08E-03	5.32E-03
XENOBIOTIC_METAB._BY_CYTOCHROME_P450	62	1.5245	3.36E-03	1.51E-02
CYTOSOLIC_DNA_SENSING_PATHWAY	52	1.5816	3.42E-03	1.51E-02
VIRAL_MYOCARDITIS	68	1.4405	4.39E-03	1.96E-02
ASCORBATE_AND_ALDARATE_METABOLISM	21	1.5205	6.20E-03	2.86E-02
NATURAL_KILLER_CELL_MEDIATED_CYTOTOX.	123	1.3730	7.22E-03	3.25E-02
STEROID_HORMONE_BIOSYNTHESIS	49	1.5533	7.94E-03	3.62E-02
CALCIUM_SIGNALING_PATHWAY	173	1.3406	9.14E-03	3.97E-02
LINOLEIC_ACID_METABOLISM	29	1.4904	1.00E-02	4.21E-02
AUTOIMMUNE_THYROID_DISEASE	48	1.5072	1.04E-02	4.21E-02
ECM_RECEPTOR_INTERACTION	84	1.4313	1.09E-02	4.53E-02

Upregulated from early senescence to late senescence (SEN-E_SEN-L_UP)

Pathway name	Size	NES	NOM p-val	FDR p-val
OLFACTORY_TRANSDUCTION	367	1.6009	<1.00E-03	<5.00E-02
CUSTOM_IFN-I	50	1.4722	<1.00E-03	<5.00E-02
NEUROACTIVE_LIGAND_RECEPTOR_INTERACT.	270	1.3253	<1.00E-03	<5.00E-02

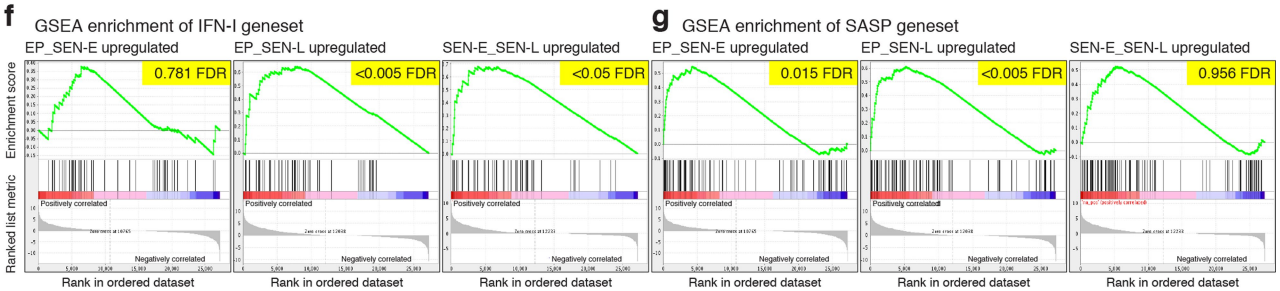

Extended Data Fig. 3 | See next page for caption.

Extended Data Fig. 3 | Evolution of transcriptomic changes during progression of cellular senescence. RNA-seq was performed on early proliferating LF1 cells and cultures at 8 weeks (SEN-E) and 16 weeks (SEN-L) in senescence (points C and D, respectively, in Extended Data Fig. 1a). Data were analysed using a three-way comparison: EP versus SEN-E, EP versus SEN-L and SEN-E versus SEN-L (see Methods for details). **a**, Area-proportional generalized Venn diagrams depicting the intersections of the three comparisons for the following datasets. **i**–**ii**, Significantly upregulated and downregulated genes (row '2×' in **b**). **iii**–**iv**, Significant KEGG pathways identified by gene set enrichment analysis (GSEA). Note the considerable evolution of the transcriptome in late senescence, exemplified by large changes (especially upregulated) in differentially expressed genes as well as pathways. **v**–**vi**, Significantly changing genes in the IFN-I and SASP gene sets (see Supplementary Table 4 for annotation of gene sets). Note that most changes in SASP genes occur early, whereas a large component of IFN-I changes is specific for late senescence. **b**, Summary of significantly changing genes using a fixed false discovery rate (FDR) (<0.05) and variable fold-change cut offs (2×, 1.75× and 1.5×). **c**, GSEA analysis of KEGG pathways. Heat map representation shows significantly upregulated pathways in red (also see **e**) and downregulated pathways in blue. Non-significant comparisons are shown in black; vertical annotations refer to Venn diagrams in **a**, **iii**–**iv**. Note that the SASP gene set is upregulated early, whereas the IFN-I gene set is upregulated late. **d**, Heat maps of significantly changing genes in the IFN-I and SASP gene sets. Vertical annotations refer to Venn diagrams in **a**, **v**–**vi**. **e**, List of significantly upregulated KEGG pathways identified using GSEA (see Supplementary Table 5 for a list of all pathways). NES, normalized enrichment scores. IFN-I and SASP gene sets are highlighted in yellow. Note the significant upregulation of IFN-I between early and late senescence. Red font identifies KEGG pathways indicative of cytosolic DNA sensing and a type I interferon response at late times. **f**, **g**, GSEA profiles of the IFN-I and SASP gene sets for all comparisons; FDR is highlighted in yellow. Note that the upregulation of IFN-I is significant for EP_SEN-L and SEN-E_SEN-L but not for EP_SEN-E, and that the upregulation of SASP is significant for EP_SEN-E and EP_SEN-L but not SEN-E_SEN-L. $n = 3$ independent biological samples. Differential expression data were analysed for significance using the GSEA GenePattern interface and the outputs were corrected for multiple comparisons by adjusting the nominal *P* values using the Benjamini–Hochberg method (see Methods for details).

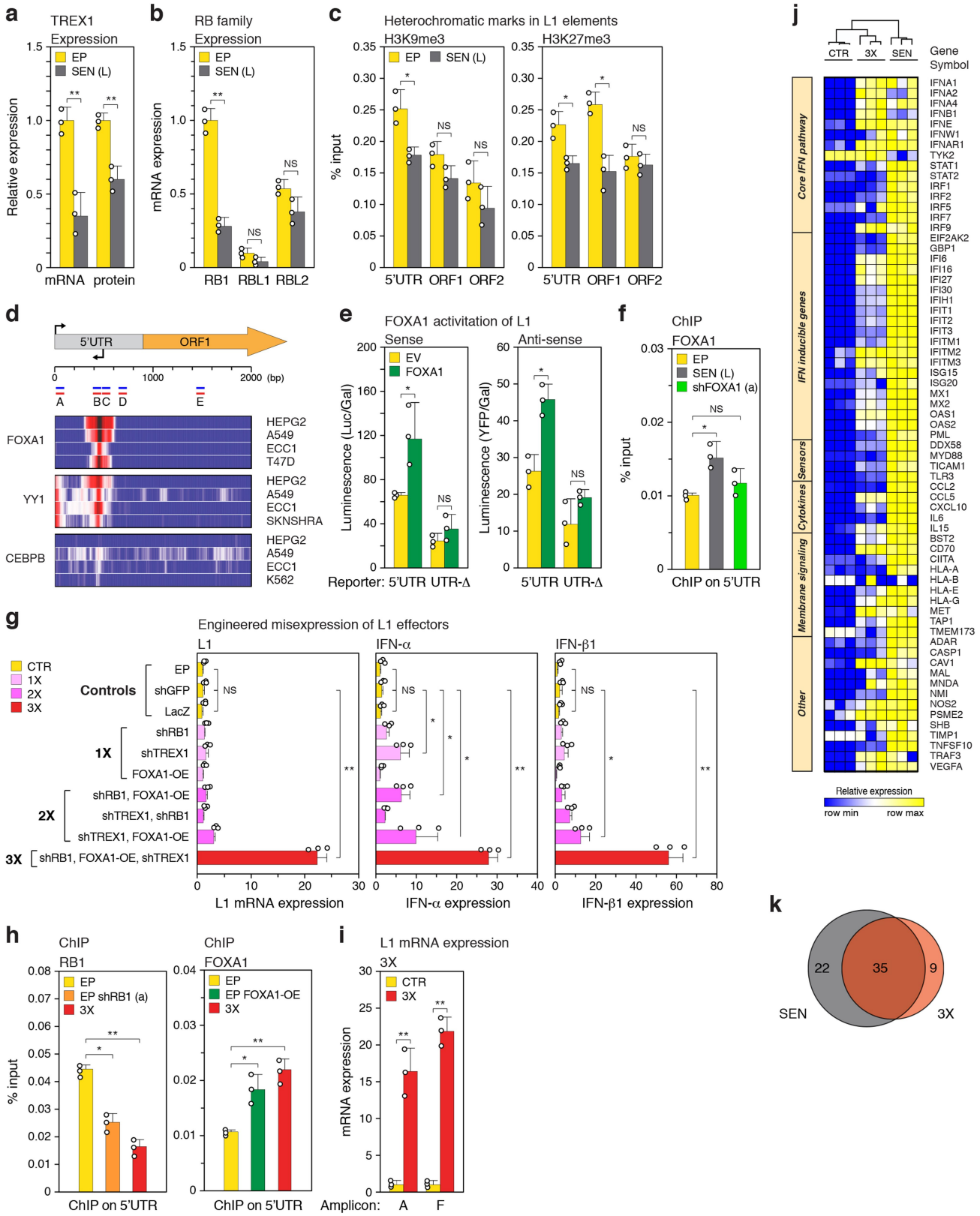

Extended Data Fig. 4 | See next page for caption.

Extended Data Fig. 4 | Characterization of L1 effectors and the IFN-I response. a, Expression of TREX1 was determined by RT–qPCR and immunoblotting. For gel source data, see Supplementary Fig. 1. **b**, Expression of RB family genes was compared by RT–qPCR. Primer pairs for all genes were verified to be of equivalent efficiency. **c**, Enrichment of H3K9me3 and H3K27me3 on L1 elements was examined by ChIP–qPCR (PCR primers illustrated in Fig. 1b were used: 5′ UTR, amplicon A; ORF1, amplicon E; ORF2, amplicon F). **d**, ChIP–seq data from ENCODE were investigated for transcription factors that bind to the L1 consensus sequence. The fold change, $\log_2$(enrichment), relative to input controls is shown for the indicated cell lines. The binding of YY1 to the L1 promoter has been documented[69] and was used as a positive control. CEBPB was used as a negative control. A schematic illustrating L1 coordinates and relevant features is shown above. Amplicons A–E are the same as shown in Fig. 1b. **e**, Transcriptional activity of the intact L1 5′ UTR or a UTR lacking the FOXA1-binding site (UTR−Δ) was determined using sense and antisense reporters cotransfected into early passage LF1 cells either with a FOXA1 expression plasmid or empty vector. **f**, FOXA1 was knocked down in senescent cells with shFOXA1 (a) (see also Fig. 2e and Extended Data Fig. 5a) and binding to the L1 5′ UTR (amplicon B) was determined by ChIP–qPCR. **g**, Knockdown of RB1, TREX1 and ectopic expression of FOXA1 were performed in early passage cells in all single (1×), double (2×) and triple (3×) combinations and assessed by RT–qPCR using poly(A)-purified RNA for activation of L1, *IFNA* and *IFNB1* expression (primers for amplicon F). Three controls are shown: cells infected with irrelevant shRNA (shGFP), expression construct (LacZ), or uninfected early passage cells. **h**, L1 5′ UTR occupancy of RB1 and FOXA1 in 3× cells was determined by ChIP–qPCR performed as in Fig. 2a, b. Primers for amplicons A and B were used for *RB1* and *FOXA1*, respectively. For comparison, single interventions in early passage cells with shRB1 (a) or *FOXA1* cDNA expression (EP FOXA1-OE) are also shown. **i**, Confirmation of full-length L1 mRNA expression in 3× cells using RT–qPCR with primers for amplicons A and F on poly(A)-purified RNA. CTR, cells infected with irrelevant shRNA (shGFP). **j**, Heat map representation showing all biological replicates for the 67 genes significantly changing expression in SEN and/or 3× cells (Fig. 2h, Supplementary Table 6). Column clustering was calculated as 1 − Pearson correlation. Rows have been grouped into functional subsets of the IFN-I response. **k**, Venn diagram showing the overlap between the 67 significantly changing genes. $n = 3$ independent biological samples, repeated in two independent experiments (**a**–**f**, **h**); $n = 3$ independent experiments (**g**, **i**).) Data are mean ± s.d. $^*P \leq 0.05$, $^{**}P \leq 0.01$, unpaired two-sided *t*-test. Exact *P* values can be found in the accompanying Source Data.

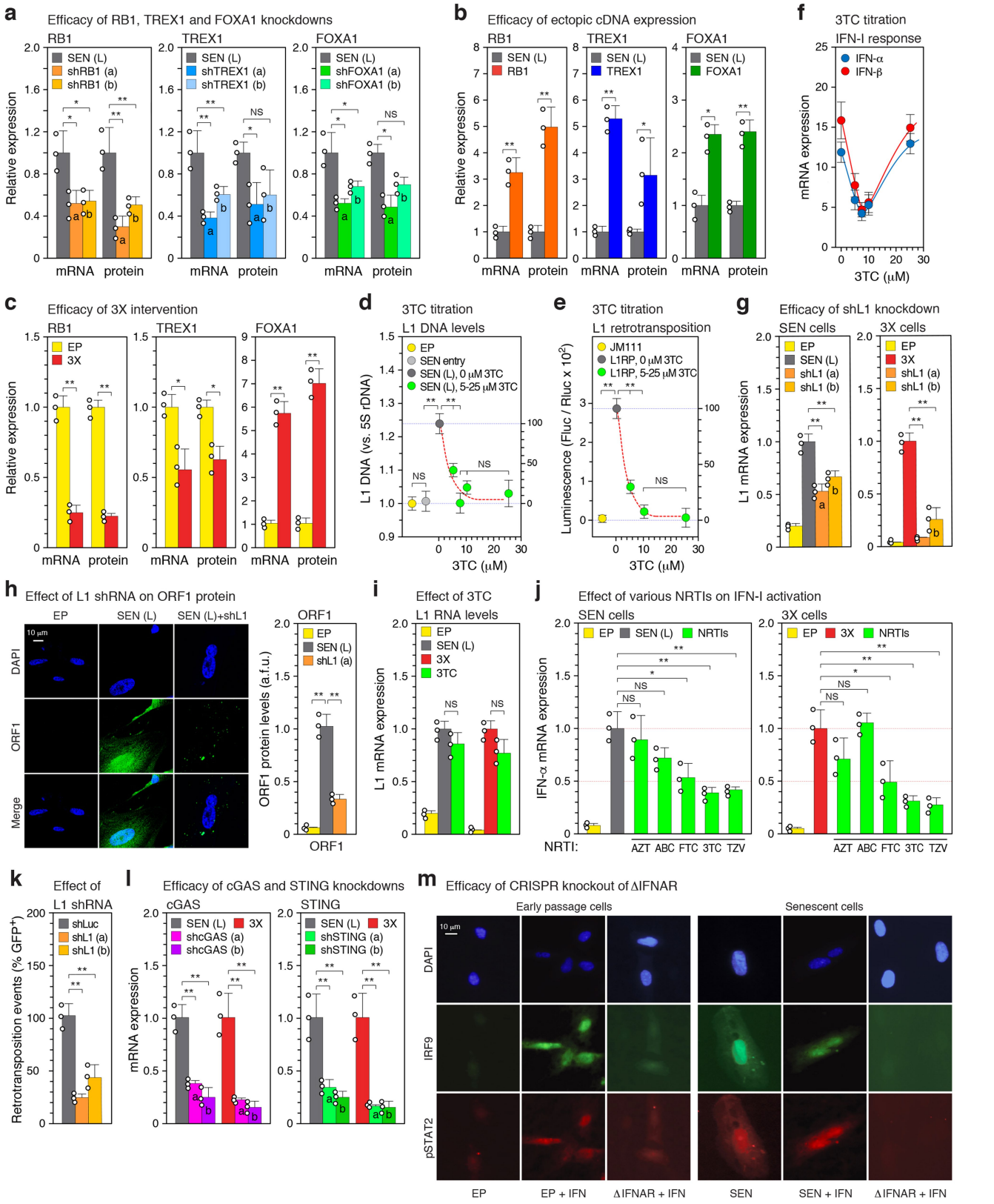

Extended Data Fig. 5 | See next page for caption.

Extended Data Fig. 5 | Efficacy of genetic and pharmacological interventions. a, **b**, Knockdowns with two distinct shRNAs (a or b) (**a**) or ectopic cDNA expression (**b**) were performed in senescent cells as described in Fig. 2d, e, g (also see Methods). The effectiveness of these manipulations on their targets was assessed by RT–qPCR and immunoblotting. For gel source data, see Supplementary Fig. 1. **c**, RB1, TREX1 and FOXA1 mRNA and protein expression after the triple (3×) intervention (Fig. 2f). **d**, The effect of 3TC treatment on the relative abundance of L1HS sequences in senescent cells was determined by multiplex TaqMan qPCR on total DNA (primer set 6, Supplementary Table 1). SEN entry, 0 weeks in senescence (Fig. 1a; point A in Extended Data Fig. 1a). 3TC was administered continuously from SEN entry until collection 16 weeks later. **e**, The dual luciferase L1 reporter system[52] was used to determine the effect of 3TC dosing on retrotransposition. L1 reporters were introduced into early passage cells using lentivirus vectors (Methods) and cells were treated with 3TC for 4 days before collection and assay. JM111, a defective reporter carrying mutations in ORF1 (absence of 3TC); L1RP, a retrotransposition competent reporter. **f**, The effect of 3TC dosing on the IFN-I response. The experiment in **d** was processed by RT–qPCR to determine the expression of *IFNA* and *IFNB1*. **g**, Knockdowns of L1 elements were performed with two distinct shRNAs (a and b) in senescent cells (as in Fig. 2d, e, g) or 3× cells (as in Fig. 2f). The effectiveness on L1 expression was assessed by RT–qPCR using poly(A)-purified RNA and primers F. **h**, Cells in the experiment in **g** were examined for levels of ORF1 protein by immunofluorescence. Image analysis was performed with CellProfiler software (Methods). More than 200 cells were examined for each condition (a.f.u., arbitrary fluorescence units). **i**, The L1 shRNA treatment in the experiment in **g** was substituted with 3TC treatment (10 μM) for the same period of time. **j**, Five different NRTIs (or combinations) were tested for effects on the IFN-I response. AZT (zidovudine, 15 μM), ABC (abacavir, 15 μM), FTC (emtricitabine, 10 μM), 3TC (10 μM) and TZV (Trizivir, a combination of 15 μM AZT, 15 μM ABC and 7.5 μM 3TC). Cells were treated for 4 weeks between 12 and 16 weeks in senescence (Fig. 1a; points D and E in Extended Data Fig. 1a). 3× cells (Fig. 2f) were treated with 3TC for 48 h after the completion of the last drug selection. *IFNA* expression was determined by RT–qPCR. **k**, A native L1 reporter (pLD143)[53] was co-transfected with shRNA plasmid vectors into HeLa cells (Methods). Retrotransposition was scored as GFP-positive cells, and shL1 knockdowns were normalized to a shLuc negative control. The absolute average retrotransposition frequency (percentage of GFP-positive cells) was 4.1, which matches the published values for the reporter used (pLD143)[53]. **l**, Knockdowns of cGAS and STING were performed in senescent or 3× cells as with the other shRNAs (as in **a**, **g**, and Fig. 2d, e, g). **m**, Downregulation of interferon signalling after CRISPR-mediated inactivation of *IFNAR1* and *IFNAR2* genes was verified by the absence of IRF9 nuclear translocation and STAT2 phosphorylation in response to interferon stimulation. Cells were infected with lentivirus vectors expressing Cas9 and gRNAs to both *IFNAR1* and *IFNAR2* (ΔIFNAR, Methods). After the infection, cells were reseeded on coverslips, treated with interferon for 2 h, and examined by immunofluorescence microscopy. The experiment was repeated three times with similar results. $n = 3$ independent experiments (**a**–**j**, **l**), $n = 3$ independent biological samples, repeated in two independent experiments (**k**). Data are mean ± s.d. $^{*}P \leq 0.05$, $^{**}P \leq 0.01$, unpaired two-sided *t*-test. Exact *P* values can be found in the accompanying Source Data.

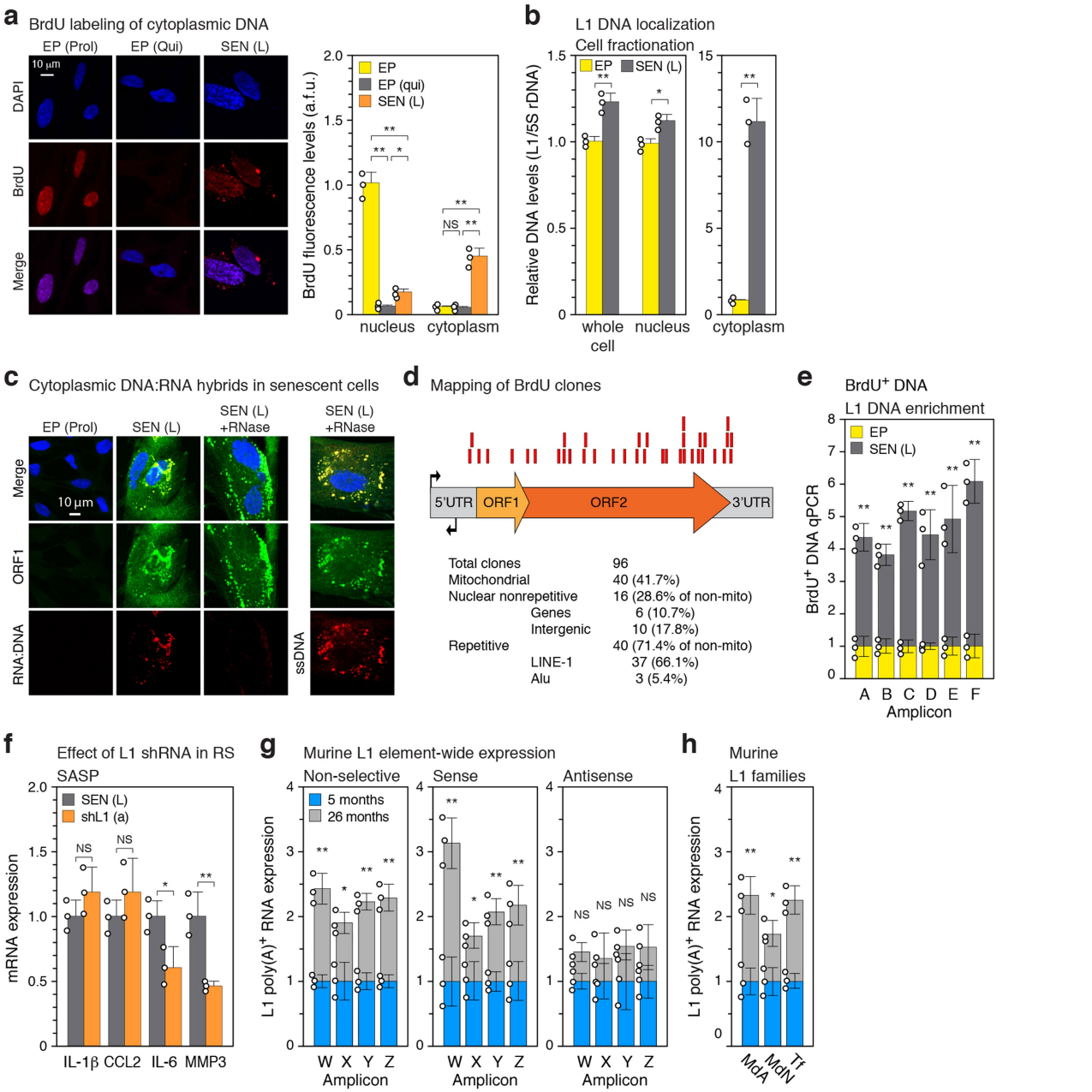

Extended Data Fig. 6 | Characterization of cytoplasmic DNA in senescent cells. a, Left, quiescent and senescent cells were treated with BrdU as in Fig. 3c and the cellular localization of BrdU incorporation was visualized by immunofluorescence microscopy. Proliferating cells (EP (Prol)) are shown as a positive control for nuclear BrdU incorporation. Right, the signals were quantified using CellProfiler software (Methods). More than 200 cells were examined for each condition. **b**, Senescent (and early passage control) cells (neither labelled with BrdU) were fractionated into nuclear and cytoplasmic fractions, and the representation of L1 sequences in these compartments (as well as whole cells) was assessed with qPCR as in Fig. 3c (TaqMan multiplex qPCR assay[16], amplicon F, Fig. 1b). Note that the *y*-axis units differ by tenfold between the left and right panels. **c**, Cells were examined by immunofluorescence microscopy for the presence of ORF1 protein, RNA–DNA hybrids, and ssDNA. See Methods and Supplementary Table 2 for antibodies. The RNA–DNA signal in senescent cells largely colocalized with the ORF1 signal and was lost after RNase A treatment. The ssDNA signal also colocalized with the ORF1 signal and was exposed by RNase treatment. The experiment was repeated three times with similar results. **d**, The pulled-down BrdU-containing DNA (**a** and Fig. 3c; Methods) was cloned and Sanger sequenced. Of the 96 total clones examined, 37 mapped to L1. Red boxes represent the relative positions of these clones on the L1 consensus sequence. **e**, Senescent cells labelled with BrdU (**a** and Fig. 3c) were immunoprecipitated with anti-BrdU antibodies, and the representation of L1 sequences in the pulled-down DNA was assessed using qPCR with primers spanning the entirety of L1 elements (Fig. 1b, c). **f**, Senescent cells were treated with L1 shRNA (using lentiviral vectors as described in Extended Data Fig. 5g) between 12 and 16 weeks of senescence, and expression of SASP genes was determined. **g**, Transcription throughout mouse L1 elements was assessed in a strand-specific manner using the same strategy as was applied to human L1 elements (Fig. 1b, c). The amplicons (designated W–Z to distinguish them from the human-specific primers) correspond to the 5′ UTR (W), ORF1 (X), ORF2 (Y) and 3′UTR (Z). See Methods and Supplementary Table 1 for primer sequences (primer sets 37 and 48–50). Poly(A) RNA was prepared from male white adipose tissue. A total of 12 mice were assessed (3 pools of 4 mice each) in 3 independent experiments. **h**, Expression of the three currently active families of mouse L1 elements (MdA, MdN and Tf). Primers were designed to distinguish 5′ UTR polymorphisms of the MdA, MdN and Tf families (Methods, Supplementary Table 1 primer sets 51–53). RT–qPCR was performed as in **f** (non-strand-specific). $n = 3$ independent biological samples, repeated in two independent experiments (**a**, **b**, **e**); $n = 3$ independent experiments (**f**). Data are mean ± s.d. $^{*}P \leq 0.05$, $^{**}P \leq 0.01$, one-way ANOVA with Tukey's multiple comparisons test (**a**), unpaired two-sided *t*-test (**b**, **e**–**h**). Exact *P* values can be found in the accompanying Source Data.

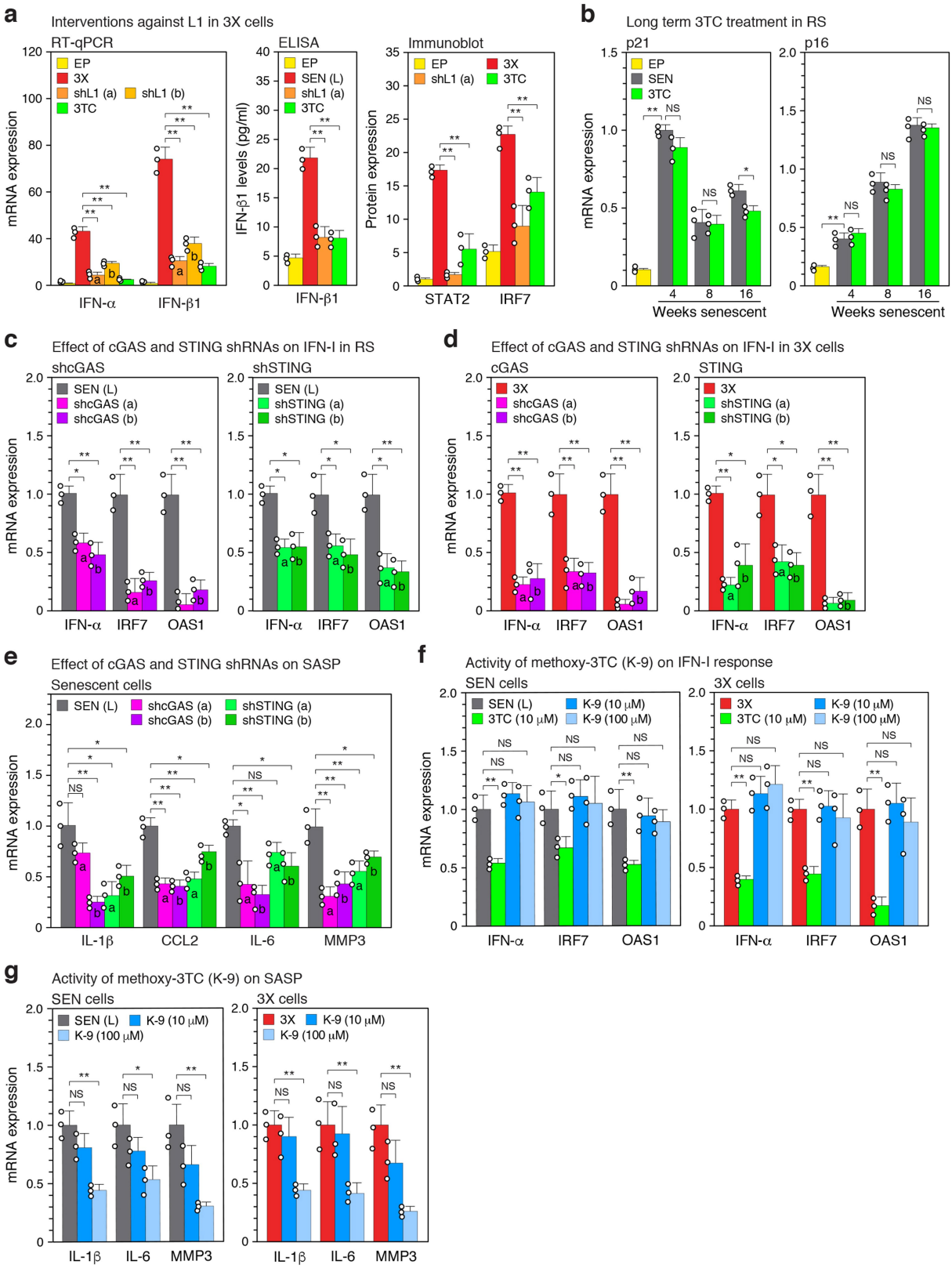

Extended Data Fig. 7 | See next page for caption.

Extended Data Fig. 7 | Effects of ablating L1 activation, the cytoplasmic DNA sensing pathway, or interferon signalling on expression of the IFN-I and SASP responses. **a**, 3× cells were treated with L1 shRNA or with 3TC for 48 h as described in Extended Data Fig. 5g,i. Effects on the IFN-I response were determined by RT–qPCR, ELISA or immunoblotting. For gel source data, see Supplementary Fig. 1. **b**, Cells were serially passaged into replicative senescence with 3TC (10 μM) present throughout, as in Fig. 3f, and expression of the CDK inhibitors *p21* and *p16* was assessed by RT–qPCR. **c**, Senescent cells were treated with shRNAs against *CGAS* or *STING* between 12 and 16 weeks of senescence (as described in Extended Data Fig. 5l), and expression of IFN-I response genes (*IFNA*, *IRF7* and *OAS1*) was determined. **d**, cGAS and STING knockdowns were performed with shRNAs in 3× cells (as in **c**), and expression of IFN-I genes was examined by RT–qPCR. **e**, cGAS and STING were knocked down in senescent cells with shRNAs (as in **c**), and expression of SASP response genes (*IL1B*, *CCL2*, *IL6* and *MMP3*) was assayed by RT–qPCR. **f**, **g**, The activity of K-9 was compared with 3TC in senescent and 3× cells. Senescent cultures were treated between 12 and 16 weeks (as in Fig. 3b) and 3× cultures for 48 h (as in **a**). Effects on the expression of IFN-I genes (*IFNA*, *IRF7* and *OAS1*) and SASP genes (*IL1B*, *IL6* and *MMP3*) was assessed by RT–qPCR. $n = 3$ independent experiments. Data are mean ± s.d. $^{*}P \leq 0.05$, $^{**}P \leq 0.01$, unpaired two-sided *t*-test. Exact *P* values can be found in the accompanying Source Data.

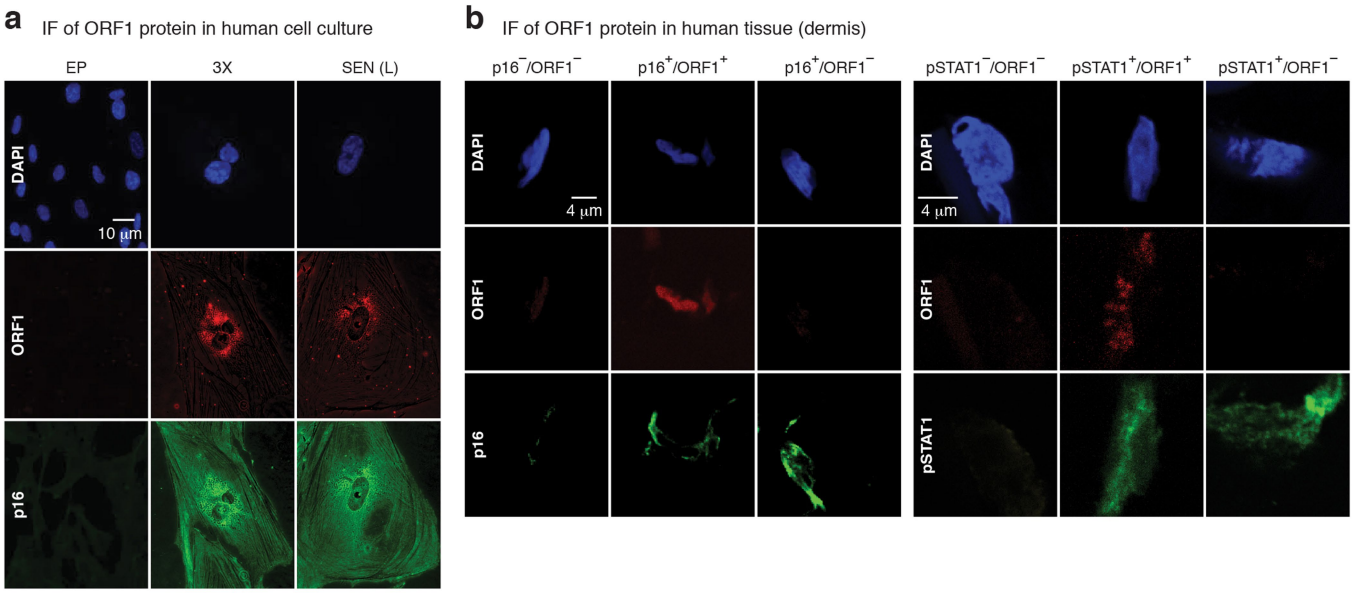

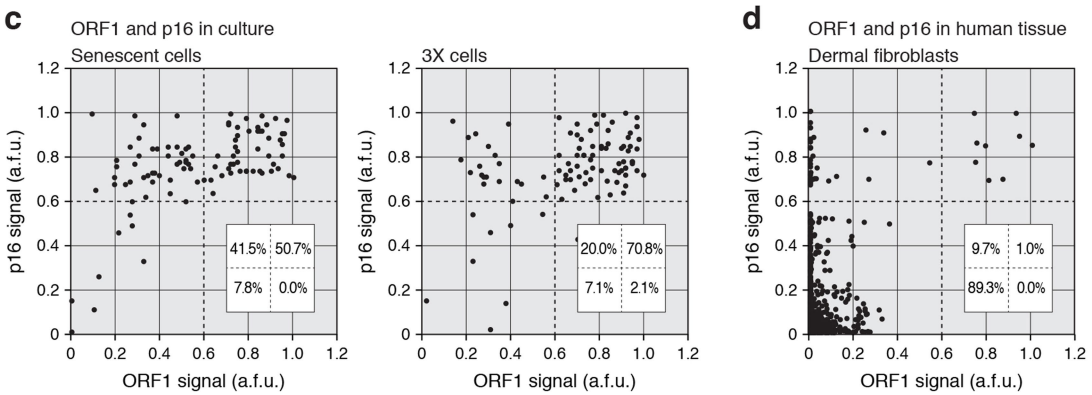

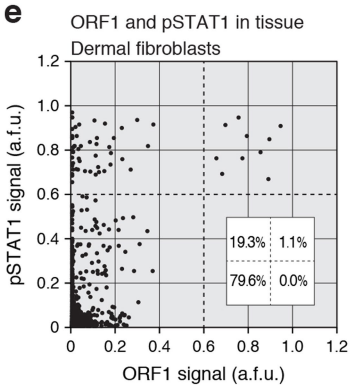

f Abundance of senescent ($p16^+$) and L1-activated ($ORF1^+$) cells

Condition	$p16^+$ as % total	$ORF1^+$ as % $p16^+$
SEN	92.2	55.0
3X	90.8	78.0
Skin	10.7	10.3

g Abundance of $pSTAT1^+$ and $ORF1^+$ cells

Condition	$pSTAT1^+$ as % total	$ORF1^+$ as % $pSTAT1^+$
Skin	20.4	5.4

h Human Subjects Summary

Subject	Sex	Age	TIF^+ (% total nuclei)	$p16^+$ (% total nuclei)
A	F	57	11.9	11.2
B	M	57	18.2	13.1
C	F	57	13.9	10.8
D	M	57	11.1	7.7
			Mean=13.8	Mean=10.7

Extended Data Fig. 8 | Assessment of p16, L1 ORF1 and pSTAT1 expression in senescent cells and skin specimens from aged humans. **a**, Immunofluorescence (IF) detection of p16 and ORF1 in early passage, 3× and senescent cells. **b**, Representative images of combinatorial ORF1 and p16 or ORF1 and phosphorylated STAT1 (pSTAT1) staining in human dermis. The experiments in **a** and **b** were repeated three times independently with similar results. **c**, Cells were plated on coverslips, stained and quantified as described in the Methods. A total of 200 cells in several fields were scored for each condition. Insets show the percentage of cells found in each quadrant. **d**, **e**, Abundance of ORF1 and p16 or pSTAT1 cells in human skin. Skin biopsies were cryosectioned and stained as described in the Methods. A total of 200 dermal fibroblast cells in several fields were scored for each subject. Aggregated data for 4 subjects (800 cells) are shown. **f**, Data in **c** and **d** were recalculated to show the relative abundance of $p16^+$ cells among all cells, and $ORF1^+$ cells in the $p16^+$ pool of cells. **g**, Data in **e** were recalculated as in **f**. **h**, Characteristics of the human subjects used in the analysis of dermal fibroblasts. These specimens were collected as part of the ongoing Leiden Longevity Study[62]. The specimens used here were chosen randomly from leftover material. The telomere dysfunction-induced foci (TIF) assay[34] relies on a two-parameter (colour) visualization of telomeres (using a FISH probe) and immunofluorescent detection of DNA damage foci (using antibody to 53BP1). Because of limiting material, it was not possible to combine detection of p16 with TIFs in a three-colour experiment.

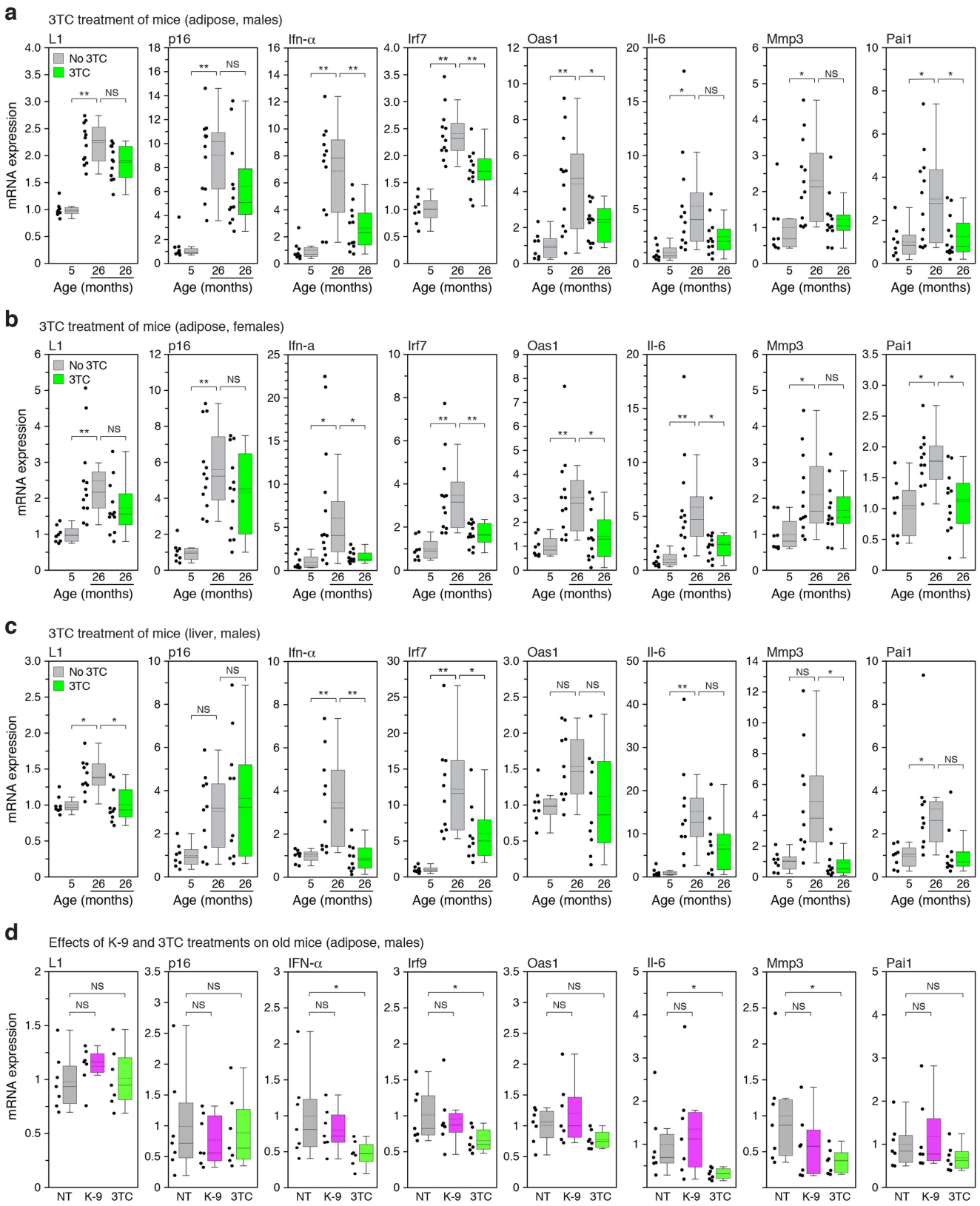

Extended Data Fig. 9 | See next page for caption.

Extended Data Fig. 9 | Effects of 3TC or K-9 treatment on L1, p16, IFN-I and SASP gene expression in mouse tissues. a–c, Mice at the indicated ages were treated with 3TC continuously for two weeks (see also Fig. 4c, e, Extended Data Fig. 10d–f and Methods). For all conditions, the expression of L1 mRNA, *p16*, three representative IFN-I response genes (*Ifna*, *Irf7* and *Oas1*) and three representative SASP genes (*Il6*, *Mmp3* and *Pai1*) were assessed by RT–qPCR. In no instance was expression at 5 months plus 3TC significantly different from the no-drug control, therefore these data are not shown in the figure (for all collected data, see Supplementary Table 7). Each point represents one animal. **a**, Visceral white adipose, male mice. $n = 8$ mice at 5 month; $n = 12$ mice at 26 months; $n = 12$ mice at 26 months + 3TC. **b**, Visceral white adipose, female mice. $n = 8$ mice at 5 months; $n = 12$ mice at 26 months; $n = 12$ mice at 26 months + 3TC. **c**, Liver, male mice. $n = 8$ mice at 5 months; $n = 10$ mice at 26 months; $n = 10$ mice at 26 months + 3TC. **d**, Mice at the age of 26 months were treated with K-9 or 3TC in drinking water for two weeks and analysed by RT–qPCR as above. NT, not treated. Visceral white adipose, male mice, $n = 7$ mice for each group. Box plots as in Fig. 4. Data are mean ± s.d. $^{*}P \leq 0.05$, $^{**}P \leq 0.01$, one-way ANOVA with Tukey's multiple comparisons test. Exact *P* values can be found in the accompanying Source Data.

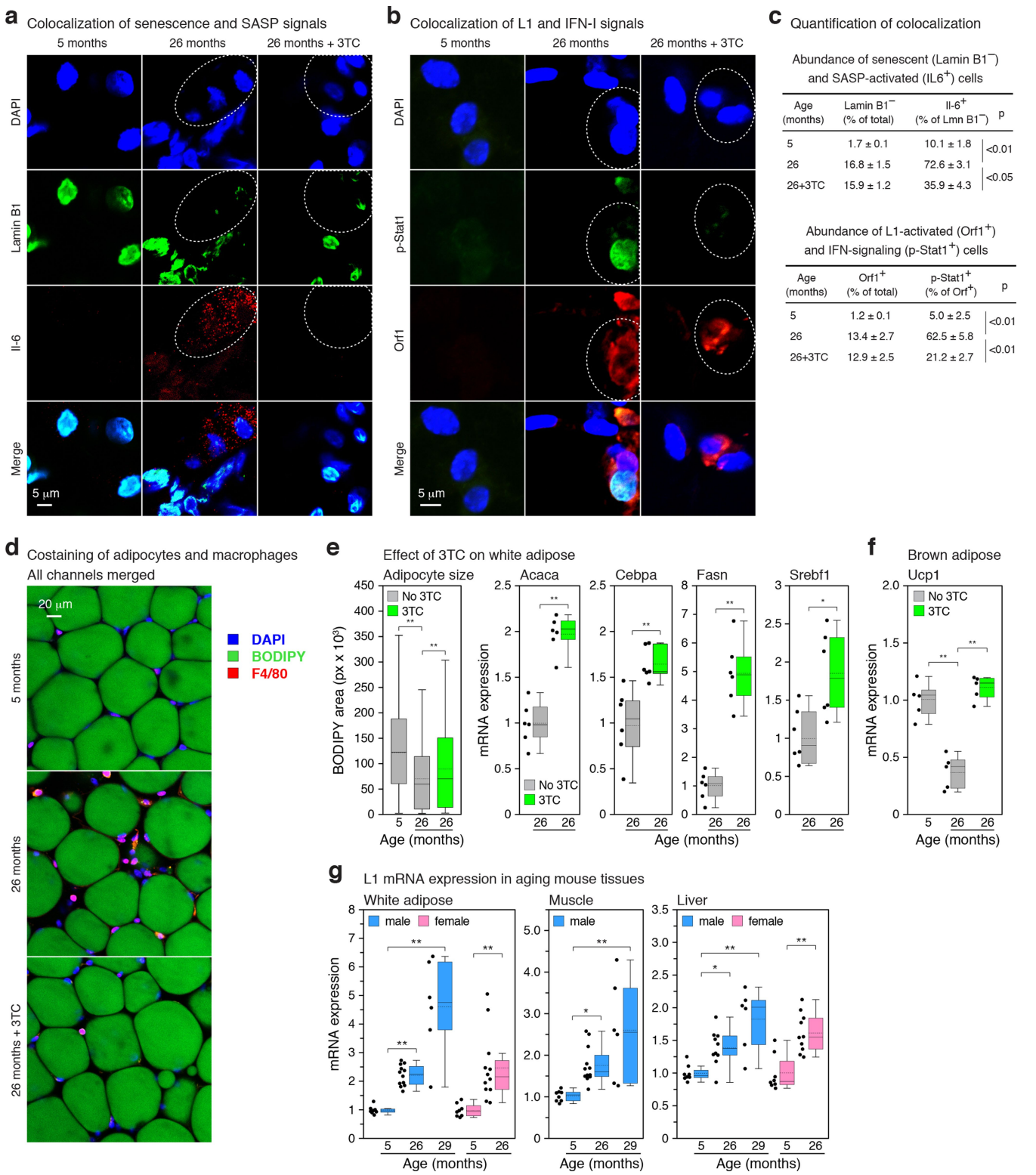

Extended Data Fig. 10 | See next page for caption.

Extended Data Fig. 10 | Combinatorial assessment of senescence, IFN-I, SASP and L1 markers and effects of 3TC on age-associated phenotypes in mouse tissues. a, **b**, Whole-mount immunofluorescence was performed on white adipose of 5- and 26-month-old male mice (with and without 2 weeks of 3TC treatment). **a**, Loss of lamin B1 (senescence marker) was colocalized with IL-6 (SASP marker). **b**, pSTAT1 (IFN-I marker) was colocalized with ORF1 (L1 marker). **c**, Quantification of the experiments in **a** and **b**. Four mice and at least 200 cells per animal were scored for each condition. **d**, Neutral lipids were stained with BODIPY to visualize mature adipocytes in whole-mount preparations, and macrophages were detected by immunofluorescence using the F4/80 antibody. **e**, The effects of 2 weeks of 3TC treatment on adipogenesis were assessed by measuring mean adipocyte size (left), and by RT–qPCR to determine the expression of key adipogenic genes (right; *Acaca*, acetyl-CoA carboxylase 1; *Cebpa*, CCAAT/enhancer-binding protein alpha; *Fasn*, fatty acid synthase; *Srebf1*, sterol regulatory element-binding protein 1). Adipocyte size (BODIPY-stained area) was calculated using CellProfiler; aggregated data for 5 mice and 500 total cells are shown. For RT–qPCR data, each point represents one animal; $n = 6$ mice. **f**, Expression of the *Ucp1* gene (thermogenin) in brown adipose tissue was determined by RT–qPCR and is represented as in **e**. $n = 5$ mice. **g**, Expression of L1 mRNA was determined by RT–qPCR and is represented as in **e**. $n = 8$ mice at 5 months; $n = 12$ mice at 26 months; $n = 6$ mice at 29 months. Box plots as in Fig. 4. Data are mean ± s.d. $^{*}P \leq 0.05$, $^{**}P \leq 0.01$, one-way ANOVA with Tukey's multiple comparisons test (**c**, **e**, left, **f**, **g**), or unpaired two-sided *t*-test (**e**, right). Exact *P* values can be found in the accompanying Source Data.

nature research

Corresponding author(s): John M. Sedivy

Reporting Summary

Nature Research wishes to improve the reproducibility of the work that we publish. This form provides structure for consistency and transparency in reporting. For further information on Nature Research policies, see Authors & Referees and the Editorial Policy Checklist.

Statistical parameters

When statistical analyses are reported, confirm that the following items are present in the relevant location (e.g. figure legend, table legend, main text, or Methods section).

n/a	Confirmed	
☐	☒	The exact sample size (*n*) for each experimental group/condition, given as a discrete number and unit of measurement
☐	☒	An indication of whether measurements were taken from distinct samples or whether the same sample was measured repeatedly
☐	☒	The statistical test(s) used AND whether they are one- or two-sided *Only common tests should be described solely by name; describe more complex techniques in the Methods section.*
☒	☐	A description of all covariates tested
☐	☒	A description of any assumptions or corrections, such as tests of normality and adjustment for multiple comparisons
☐	☒	A full description of the statistics including central tendency (e.g. means) or other basic estimates (e.g. regression coefficient) AND variation (e.g. standard deviation) or associated estimates of uncertainty (e.g. confidence intervals)
☐	☒	For null hypothesis testing, the test statistic (e.g. *F*, *t*, *r*) with confidence intervals, effect sizes, degrees of freedom and *P* value noted *Give P values as exact values whenever suitable.*
☒	☐	For Bayesian analysis, information on the choice of priors and Markov chain Monte Carlo settings
☒	☐	For hierarchical and complex designs, identification of the appropriate level for tests and full reporting of outcomes
☒	☐	Estimates of effect sizes (e.g. Cohen's *d*, Pearson's *r*), indicating how they were calculated
☐	☒	Clearly defined error bars *State explicitly what error bars represent (e.g. SD, SE, CI)*

Our web collection on statistics for biologists may be useful.

Software and code

Policy information about availability of computer code

Data collection	Collection of qPCR data: ExpressionSuite Software by Applied Biosystems, version 1.2.3. Microscope imaging: confocal, ZEN Black Edition SP1 by Carl Zeiss, version 8.1. Fluorescence, NIS Elements by Nikon, version 4.50. Brightfield, AxioVision by Carl Zeiss, version 4.8.2 SP3. Immunoblot Imaging: Image Studio by LI-COR Biosciences, version 5.2. ELISA plate reader: SoftMax® Pro software by Molecular Devices, version 5.0.1. Luciferase reporter assays: Modulus Fluorometer by Turner Biosystems, version 1.3

Data analysis	Excel was used to perform general statistical analyses (means, s.d., t-tests, etc). For 1-way ANOVA and Tukey's post-hoc test R software for statistical computing (64-bit version 3.3.2) was used. For RNAseq data analyses, the following software were used: Bowtie, HiSat2, featureCounts, EdgeR, RepEnrich and the GenePattern interface for GSEA Preranked. To detect and annotate L1 elements the web front-end L1Xplorer was used. GeneGlobe Data Analysis by Qiagen was used to analyze PCR array data. CellProfiler (version 2.1.1) by Broad Institute was used for image analysis. ImageJ (version 1.50i) was used for western blot quantification.

For manuscripts utilizing custom algorithms or software that are central to the research but not yet described in published literature, software must be made available to editors/reviewers upon request. We strongly encourage code deposition in a community repository (e.g. GitHub). See the Nature Research guidelines for submitting code & software for further information.

Data

Policy information about availability of data

All manuscripts must include a data availability statement. This statement should provide the following information, where applicable:

- Accession codes, unique identifiers, or web links for publicly available datasets
- A list of figures that have associated raw data
- A description of any restrictions on data availability

Sequencing data that support the findings of this study are available in GEO with the primary accession code GSE109700. All source data and exact P values (if applicable) for every figure are included in the supporting information that accompanies the paper.

Field-specific reporting

Please select the best fit for your research. If you are not sure, read the appropriate sections before making your selection.

☒ Life sciences ☐ Behavioural & social sciences ☐ Ecological, evolutionary & environmental sciences

For a reference copy of the document with all sections, see nature.com/authors/policies/ReportingSummary-flat.pdf

Life sciences study design

All studies must disclose on these points even when the disclosure is negative.

Sample size	The nature and size of all samples are described in figure legends for all experiments. Sample sizes used were based on previously published experiments and experience from the Sedivy lab. No statistical test was used to pre-determine sample size.
Data exclusions	No pre-set criterion or data exclusion was used.
Replication	Results shown are representative of several independently performed experiments. Number of biological replicates and independent experiments is described in figure legends. All attempts at replication were successful. There were no findings that were not replicated or could not be reproduced.
Randomization	Genotype of C57BL/6 mice is known to investigators. No pre-established selection criteria for mice were used, other than gender and ages. When mice with desired gender were at appropriate ages, all mice in corresponding cages were used. No selection criteria were applied. Animals were assigned randomly to cohorts (drug-treated, control) by a technician that was blinded to the appearance or other characteristics of the animals.
Blinding	The investigators were blinded when quantifying IF results. Fields or sections of tissues for quantification were randomly selected and scored, as indicated in Methods. The investigators were also blinded when scoring glomerulosclerosis and muscle fiber diameter.

Reporting for specific materials, systems and methods

Materials & experimental systems

n/a	Involved in the study
☐	☒ Unique biological materials
☐	☒ Antibodies
☐	☒ Eukaryotic cell lines
☒	☐ Palaeontology
☐	☒ Animals and other organisms
☐	☒ Human research participants

Methods

n/a	Involved in the study
☒	☐ ChIP-seq
☒	☐ Flow cytometry
☒	☐ MRI-based neuroimaging

Unique biological materials

Policy information about availability of materials

Obtaining unique materials

Kamuvudine-9 (Ref. Ambati, J.,Fowler, B. & Ambati, K. Compositions and Methods for Treating Retinal Degradation. PCT Patent Publication WO/2016/138425 (2016)) is available upon reasonable request from Dr. J. Ambati.

Antibodies

Antibodies used

Immunoblotting – GAPDH – (Cell Signaling Technology, Rabbit, cat.no. 5174, clone: n/a, 1:5000)
Immunoblotting – GAPDH – (Sigma, Mouse, cat.no. G8795, clone: n/a, 1:5000)
Immunoblotting – p16 – (Santa Cruz, Mouse, cat.no. sc-1661, clone: F-12, 1:1000)
Immunoblotting – p21 – (Santa Cruz, Rabbit, cat.no. sc-756, clone: H-164, 1:1000)
Immunoblotting, ChIP – RB1 – (BD Biosciences, Mouse, cat.no. 554136, clone: G3-245, 1:1000 WB, 1:50 ChIP)
Immunoblotting – TREX1 – (Cell Signaling Technology, Rabbit, cat.no. 12215, clone: n/a, 1:1000)
Immunoblotting – FOXA1 – (Abcam, Rabbit, cat.no. ab170933, clone: EPR10881, 1:1000)
Immunoblotting – STAT2 – (Cell Signaling Technologies, Rabbit, cat.no. 4594, clone: n/a, 1:1000)
Immunoblotting – IRF7 – (Abcam, Rabbit, cat.no. ab109255, clone: EPR4718, 1:1000)
ChIP – FOXA1 – (Abcam, Goat, cat.no. ab5089, clone: n/a, 1:50)
Immunofluorescence – p16 – (Santa Cruz, Mouse, cat.no. sc-56330, clone: JC8, 1:100)
Immunofluorescence – Phospho-STAT1 – (Santa Cruz, Mouse, cat.no. sc-8394, clone: A-2, 1:50)
Immunofluorescence – Phospho-STAT2 – (Millipore, Rabbit, cat.no. 07-224, clone: n/a, 1:50)
Immunofluorescence – IRF9 – (Novus Biologicals, Rabbit, cat.no. NBP2-16991, clone: n/a, 1:100)
Immunofluorescence, Immunoprecipitation – BrdU – (BD Biosciences, Mouse, cat.no. 555627, clone: 3D4, 1:100)
Immunofluorescence – p-H2A.X – (Millipore, Mouse, cat.no. 05-636, clone: JBW301, 1:100)
Immunofluorescence – F4/80 – (Abcam, Rat, cat.no. ab6640, clone: CI:A3-1, 1:200)
Immunofluorescence – ssDNA – (Enzo, Mouse, cat.no. ALX-804-192, clone: F7-26, 1:100)
Immunofluorescence – DNA:RNA – (Kerafast, Mouse, cat.no. ENH001, clone: S9.6, 1:100)
Immunofluorescence – LaminB1 – (Santa Cruz, Goat, cat.no. sc-6216, clone: C-20, 1:200)
Immunofluorescence – IL-6 – (Cell Signaling Technologies, Rabbit, cat.no. 12912, clone: D5W4V, 1:200)
Immunofluorescence – Human LINE-1 ORF1 – (Gift of K.H. Burns, Johns Hopkins)
Immunofluorescence – Mouse LINE-1 Orf1 – (J.D. Boeke, abEA02, RabMAb clone: NYU-2-1_2)

Validation

With the exception of LINE-1 ORF1 antibodies, all antibodies are from commercially available sources and have been validated from the manufacturer with supporting publications found on manufacturer websites. Antibodies were further validated in-house using relevant positive and negative controls.

The human LINE-1 ORF1 antibody was validated in the lab of K.H. Burns, Johns Hopkins, as described in Rodic et al. Am. J. Pathol. 184, 1280-6 (2014).

The mouse LINE-1 Orf1 antibody was developed and validated in the lab of J.D. Boeke by transfection experiments and peptide blocking.

See below for summary of commerically available antibodies:
Immunoblot – p16 – Santa Cruz, sc-1661
Species: Human, Mouse, Rat
Application: ELISA, Immunocytochemistry, Immunofluorescence, Immunohistochemistry, Western Blot

Immunoblot – p21 – Santa Cruz, sc-756
Species: Mouse, Rat and Human
Application: ELISA, Immunoprecipitation, Immunofluorescence, Western Blot

Immunoblot, ChIP – RB1 – BD Biosciences, 554136
Species: Human, Mouse, Rat, Monkey, Quail, Mink (Reported)
Application: Western blot, Intracellular staining (flow cytometry), Bioimaging, Immunohistochemistry-formalin, Immunoprecipitation, Immunohistochemistry-frozen

Immunoblot – TREX1 – Cell Signaling Technologies, 12215

Species: Human
Application: Western blot

Immunoblot – FOXA1 – Abcam, ab170933
Species: Human, Mouse, Rat
Application: Western blot, Intracellular staining (flow cytometry), Bioimaging, Immunohistochemistry-formalin, Immunohistochemistry-frozen

Immunoblot – STAT2 – Cell Signaling Technologies, 4594
Species: Human
Application: Western blot

Immunoblot – IRF7 – Abcam, ab109255
Species: Human, Mouse, Rat
Application: Western blot, Intracellular staining (flow cytometry), Immunofluorescence, Immunohistochemistry-formalin, Immunoprecipitation, Immunohistochemistry-frozen

ChIP – FOXA1 – Abcam, ab5089
Species: Human, Mouse
Application: ChIP, Western blot, Immunohistochemistry-formalin, Immunoprecipitation

Immunofluorescence – p16 – Santa Cruz, sc-56330
Species: Human
Application: Western blot, Immunofluorescence, Immunohistochemistry, Immunoprecipitation, solid-phase ELISA

Immunofluorescence – p-STAT1 – Santa Cruz, sc-8394
Species: Human, Mouse and Rat
Application: Western blot, Immunofluorescence, Immunoprecipitation, Flow-cytometry, solid-phase ELISA

Immunofluorescence – p-STAT2 – Millipore, 07-224
Species: Human, Mouse
Application: Western blot, Immunofluorescence, Immunoprecipitation

Immunofluorescence – IRF9 – Novus Biologicals, NBP2-16991
Species: Human, Monkey
Application: Western blot, Immunofluorescence, solid-phase ELISA, Immunohistochemistry

Immunofluorescence, Immunoprecipitation – BrdU – BD Biosciences, 555627
Species: Human
Application: Flow cytometry, Immunofluorescence, Immunoprecipitation, Immunohistochemistry

Immunofluorescence – IRF9 – Novus Biologicals, NBP2-16991
Species: Human, Monkey
Application: Western blot, Immunofluorescence, solid-phase ELISA, Immunohistochemistry

Immunofluorescence - p-H2A.X – Millipore, 05-636
Species: Vertebrates
Application: Immunocytochemistry, Immunofluorescence, Western Blot, ChIP, Immunohistochemistry

Immunofluorescence – F4/80 – Abcam, ab6640
Species: Mouse
Application: Immunocytochemistry, Immunofluorescence, Western Blot, Radioummunoassay, Immunohistochemistry

Immunofluorescence – ssDNA – Enzo Life Sciences, F7-26
Species: Species Independent
Application: Flow Cytometry, Immunocytochemistry, Immunofluorescence, Immunohistochemistry

Immunofluorescence – RNA:DNA – Kerafast, S9.6
Species: Species Independent
Application: Dot Blot, Affinity Binding Assay, ChIP, Immunocytochemistry, Immunofluorescence, Immunohistochemistry, Immunoprecipitation

Immunofluorescence – Lamin B1– Santa Cruz, sc-6216
Species: Human, Mouse and Rat
Application: Western Blot, Immunoprecipitation, Immunofluorescence, Immunohistochemistry, solid-phase ELISA

Immunofluorescence – IL-6 – Cell Signaling Technologies, 12912
Species: Mouse
Application: Western Blot, Immunoprecipitation, Immunofluorescence, Flow cytometry

Eukaryotic cell lines

Policy information about cell lines

Cell line source(s)	LF1 cells were derived from embryonic lung tissue as described (Brown et al., Science, 1997). These cells have been in continuous use in our laboratory since their isolation in 1996. IMR-90 and WI-38 cells were obtained from the ATCC. HeLa cells were also obtained from the ATCC. 293T cells were only used for lentiviral packaging, and were obtained from Clontech.
Authentication	LF1 fibroblasts were authenticated by in-depth genome-wide sequencing analyses. IMR-90, WI-38, HeLa, and 293T cell lines were obtained from the sources above and used at low passage. They were not further authenticated.
Mycoplasma contamination	All cell cultures were periodically tested for mycoplasma. All cell lines tested negative for mycoplasma contamination.
Commonly misidentified lines (See ICLAC register)	None of these cell lines are listed in the International Cell Line Authentication Committee (ICLAC) database.

Animals and other organisms

Policy information about studies involving animals; ARRIVE guidelines recommended for reporting animal research

Laboratory animals	C57BL/6 mice were purchased from the Aged Rodent Colonies operated by the National Institute on Aging. Mice of both sexes were obtained at 5 and 18 months of age. The 5 month old animals were sacrificed after a short (1 week) acclimatization period. The 18 month old animals were housed until they reached a desired age. Mice were fed ad libitum on a regular diet, and handled following institutional regulations and guidelines. Both sexes were included in the study.
Wild animals	The study did not involve wild animals.
Field-collected samples	The study did not involve field-collected samples.

Human research participants

Policy information about studies involving human research participants

Population characteristics	Human skin specimens were collected as part of the Leiden Longevity Study (Schoenmaker, M. et al., Eur. J. Hum. Genet., 2006) and were provided by P. Eline Slagboom, Leiden University Medical Centre, Netherlands. 420 families of Caucasian origin took part in the Leiden Longevity Study (LLS). This group consisted of 991 long-lived brothers and/or sisters, their children and partners of their children. The samples were collected as 4 mm thickness full depth punch biopsies, embedded in optimal cutting compound (OCT), flash frozen, and stored at -80°C. Samples were shipped on dry ice to Brown University. The Brown investigators were blinded to everything except the age and sex of the subjects
Recruitment	The men were considered to be long-lived if they were 89 years or older, and the women if they were 91 years or older. Families were invited to participate when there were at least two long-lived brothers and/or sisters alive. Informed consent was obtained and all protocols were approved by the ethical committee of the Leiden University Medical Centre. The results of this study are purely observational and are not affected by any bias in cohort recruitment.